Miner Deposita
DOI 10.1007/s00126-009-0249-z

ARTICLE

Organic and inorganic geochemistry of Ljubija siderite deposits, NW Bosnia and Herzegovina

Sabina Strmić Palinkaš · Jorge E. Spangenberg · Ladislav A. Palinkaš

Received: 30 April 2008 / Accepted: 1 June 2009

Abstract The Ljubija siderite deposits, hosted by a Carboniferous sedimentary complex within the Inner Dinarides, occur as stratabound replacement-type ore bodies in limestone blocks and as siderite–sulfides veins in shale. Three principal types of ore textures have been recognized including massive dark siderite and ankerite, siderite with zebra texture, and siderite veins. The ore and host rocks have been investigated by a combination of inorganic (major, trace, and rare earth element concentrations), organic (characterization of hydrocarbons including biomarkers), and stable isotope geochemical methods (isotope ratios of carbonates, sulfides, sulfates, kerogen, and individual hydrocarbons). New results indicate a marine origin of the host carbonates and a hydrothermal–metasomatic origin of the Fe mineralization. The differences in ore textures (e.g., massive siderite, zebra siderite) are attributed to physicochemical variations (e.g., changes in acidity, temperature, and/or salinity) of the mineralizing fluids and to the succession and intensity of replacement of host limestone. Vein siderite was formed by precipitation from hydrothermal fluids in the late stage of mineralization. The equilibrium fractionation of stable isotopes reveals higher formation temperatures for zebra siderites (around 245°C) then for siderite vein (around 185°C). Sulfur isotope ratios suggest Permian seawater or Permian evaporites as the main sulfur source. Fluid inclusion composition confirms a contribution of the Permian seawater to the mineralizing fluids and accord with a Permian mineralization age. Organic geochemistry data reflect mixing of hydrocarbons at the ore site and support the hydrothermal–metasomatic origin of the Ljubija iron deposits.

Keywords Siderite · Hydrothermal–metasomatic · Major and trace elements · Stable isotopes · Organic geochemistry · Dinarides · Bosnia and Herzegovina

Editorial handling: P. Williams

S. S. Palinkaš · L. A. Palinkaš (✉)
Department of Mineralogy and Petrography, Faculty of Science,
University of Zagreb,
Horvatovac bb,
10000 Zagreb, Croatia
e-mail: lpalinkas@geol.pmf.hr

J. E. Spangenberg
Institute of Mineralogy and Geochemistry,
University of Lausanne,
Building Anthropole,
1015 Lausanne, Switzerland

Introduction

The siderite deposits at Ljubija (44.55° N, 16.3° E) are located 180 km NW of Sarajevo, Bosnia and Herzegovina. The deposits are situated at the margin of a Mesozoic carbonate platform within the Sana–Una River Paleozoic terrain of the Inner Dinarides (Fig. 1).

The history of mining in this area can be dated back to sixth century BC from remnants of historic excavations, mining equipment, and tools found. Industrial production commenced in 1916. Besides iron, several other commodities such as zinc, lead, barite, and fluorite were exploited. The Ljubija ore field includes four opencast mines (Adamuša, Tomašica, Omarska, and Vidrenjak) in an area of about 200 km^2 (Fig. 2a). The potential reserves of iron ore have been estimated to 500 million metric tons of ore grading 40–49 wt.% Fe (Grubić and Cvijić 2003).

The Fe ore occurs as stratabound siderite and ankerite replacement-type bodies in limestones and as siderite–sulfides veins within shales. Similar siderite deposits

Published online: 18 July 2009

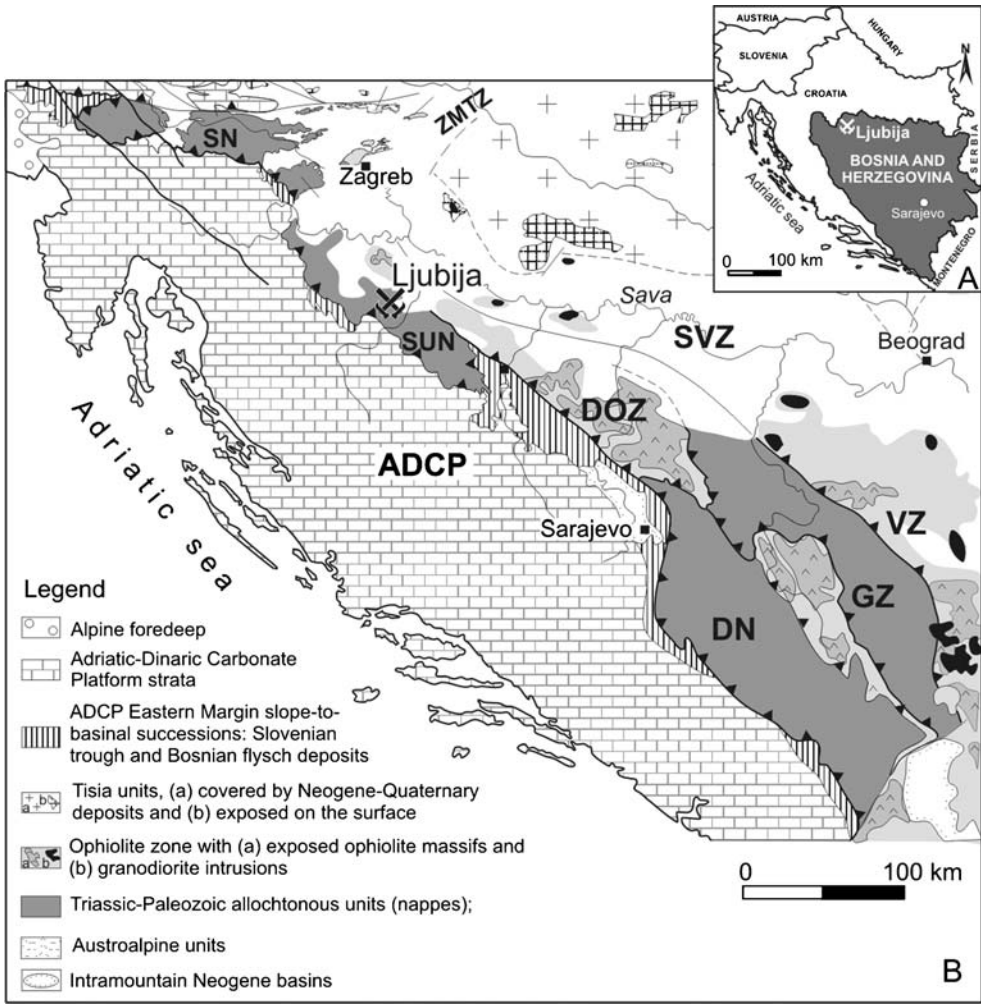

Fig. 1 Locality maps. **a** Geographical setting of the Ljubija ore deposits. **b** Geological sketch map of the Dinarides and surrounding area (after Tomljenović 2002). *ADCP* adriatic–dinaric carbonate platform units, *DOZ* Dinaric Ophiolite Zone, *SVZ* Sava-Vardar Zone, *VA* Vardar Zone, *ZMTZ* Zagorje-Mid-Transdanubian Zone, *DN* Durmitor Nappe, *GZ* Golija Zone, *SN* Sava Nappe, *SUN* Sana–Una nappe

associated with marine carbonate rocks are known from Europe and North Africa, such as Steirischer Erzberg in Austria, Batère in France, Bakal in Russia, Sierra Menera and Marquesado in Spain, Ouenza in Algeria, and Djerissa and Hameima in Tunisia (Frimmel 1988; Laube et al. 1995; Prochaska 2000; Pohl et al. 1986; Ellmies et al. 1999; Bouzenoune and Lécolle 1997; Fernández-Nieto et al. 2003; Torres-Ruiz 2006).

There has been a long-lasting debate about on the timing and mode of formation of this type of mineralization within the Ljubija ore field. In general, there have been two major hypotheses involving either Hercynian or Alpine metallogeny and age of mineralization from Middle Carboniferous to Middle Triassic. The genesis of the Ljubija deposits has been attributed to hydrothermal replacement (Katzer 1925; Cissarz 1951) or to synsedimentary processes (Jurković 1961; Jurić 1971; Šarac 1981). More recently, it has been suggested that the deposits formed by deep circulation of Permian seawater related to an early intracontinental Tethyan rifting (Palinkaš 1988; 1990; Borojević Šoštarić 2004). On the basis of fluid inclusion studies and lead isotopes applied to siderite–barite–sulfides mineral deposits hosted by Upper Palaeozoic sedimentary complexes of the Dinarides, Palinkaš (1988, 1990) and Palinkaš et al. (2003) proposed the presence of a subterrestrial hydrothermal convection cell in the genetic model and suggested that mineralization was related to the Permian early intracontinental Tethyan rifting processes.

This paper presents the results of a detailed geochemical study of the Ljubija deposits, combining major, trace, and rare earth element (REE) analyses of carbonates, Rock Eval pyrolysis, stable isotope composition of carbonates ($^{13}C/^{12}C$, $^{18}O/^{16}O$), sulfur minerals ($^{34}S/^{32}S$), kerogens ($^{13}C/^{12}C$, $^{15}N/^{14}N$), individual hydrocarbons ($^{13}C/^{12}C$), and distribution of hydrocarbon biomarkers. The new geochemical data are used to unravel details of the formation and age of Fe mineralization at Ljubija and to estimate the relationship between organic matter alteration and ore formation. This study contributes to a better

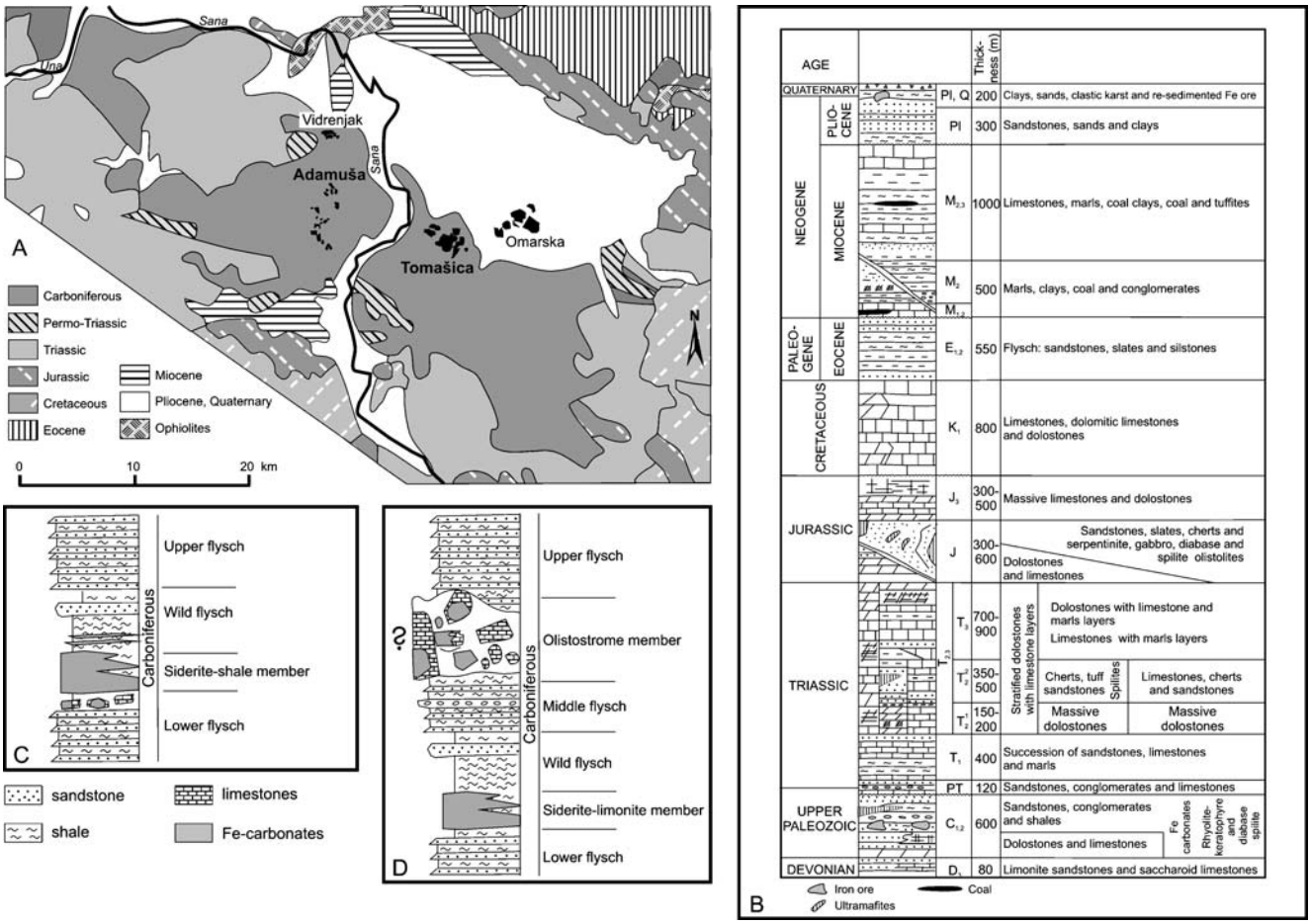

Fig. 2 Geological setting of the Ljubija ore district. **a** Geological map of the Sana–Una Palaeozoic with the location of the four open-cast mines (Adamuša, Tomašica, Omarska, and Vidrenjak) within the Ljubija ore deposits. **b** Stratigraphic column of the Sana–Una Palaeozoic terrain (after Đerković et al. 1976). **c** Stratigraphic column of Adamuša open-cast. **d** Stratigraphic column of Tomašica open-cast mine (after Grubić and Cvijić 2003)

understanding of the origin of siderite deposits related to the early stage of rifting in the Tethyan realm.

Geologic setting

The Ljubija deposits are located within the Sana–Una River Paleozoic nappe thrusted onto the Internal Dinarides (Fig. 1). Despite their complex fold, thrust, and imbricate structure, the central Dinarides are characterized by a regular zonal pattern of Mesozoic–Palaeogene tectonostratigraphic units. These units developed during the Alpine evolution of the Dinaridic part of the Tethys. From southwest to northeast, the following tectonostratigraphic units can be distinguished: (1) the Adriatic–Dinaridic carbonate platform, (2) carbonate–clastic sedimentary rocks with locally flysch signature corresponding to the passive continental margin of the Dinaridic Tethys ocean, (3) ophiolites and genetically related sedimentary formations from the Tethyan open-ocean realm, and (4) sedimentary, igneous and metamorphic units of the Eurasian active continental margin (Pamić 1993).

The northeastern and central part of the Sana–Una River Paleozoic complex was thrust onto the Mesozoic formations (Fig. 2a). The Sana–Una River terrain comprises Devonian to Quaternary sedimentary rocks (Fig. 2b) and hosts the iron carbonate deposits exclusively within the Lower and Middle Carboniferous part of the sequence (Jurić 1971).

The Ljubija deposits are placed within the Javorik flysch formation, which is well exposed within the Adamuša and the Tomašica opencast mines (Grubić et al. 2000; Grubić and Cvijić 2003; Fig. 2c, d). At Adamuša, the upper part of the lower flysch horizon contains irregular limestone blocks. Siderite with zebra texture and sparry ankerite occur mostly within the siderite–shale horizon (Fig. 2c). The Javorik flysch formation at the Tomašica opencast mine is represented by six horizons (Fig. 2d). The siderite–limonite horizon contains dark-gray massive to yellowish

coarse-grained siderite and a gossan made of porous limonite. The olistostrome horizon comprises a wide variety of carbonates including dark massive limestones, dolomitic limestones, dolostones, Fe-enriched limestones, dark massive ankerite, and dark massive siderite locally weathered to porous limonite.

Palinkaš (1988) recognized three major types of iron ore textures namely (1) dark massive siderite and ankerite, (2) zebra siderite composed of dark massive and light sparry siderite bands, and (3) sparry siderite veins hosted by shale (Fig. 3).

A simplified paragenetic sequence of the Ljubija deposits is shown in Fig. 4. Dark massive siderite and ankerite occur as replacements within limestone and dolostone blocks. The contacts between Fe carbonates and host carbonates are obscure. All carbonates mentioned above are dark gray in color due to presence of organic matter. White calcite veins a few millimeters thick crosscut dark limestones (Fig. 3a) and are more abundant near the Fe deposits. Similar yellowish siderite and white calcite veins locally intersect the dark siderite. White sparry ankerite rarely occurs at the contact with dark massive siderite. Zebra siderite is characterized by alternation of dark massive and light sparry siderite bands (Fig. 3b). Cavities infilled with white sparry ankerite, quartz, sulfides, and secondary phyllosilicates are common. Sparry siderite veins hosted by shale represent the latest phase of mineralization and contain centimeter scale yellowish to brownish siderite. The contact between siderite and shale is marked by the presence of sulfides, mainly chalcopyrite (Fig. 3c).

In the eastern part of the Ljubija ore field economically important amounts of galena, tetrahedrite, chalcopyrite, and sphalerite were exploited in the past. Barite and fluorite are present mainly as E–W oriented veins that crosscut the dolostones of the Vidrenjak opencast mine (Palinkaš 1988).

Previous geochemical studies

Fluid inclusions have been studied within the three major ore texture types (Palinkaš 1988; Borojević Šoštarić 2004). Fluid inclusions in quartz associated with dark massive siderite are of NaCl-$CaCl_2$-H_2O composition, have low to moderate salinities (2.0–23.0 wt.% NaCl equ) with a homogenization temperatures (T_h) between 80°C and 160°C. Zebra siderite is characterized by inclusions with NaCl-$CaCl_2$-H_2O composi-

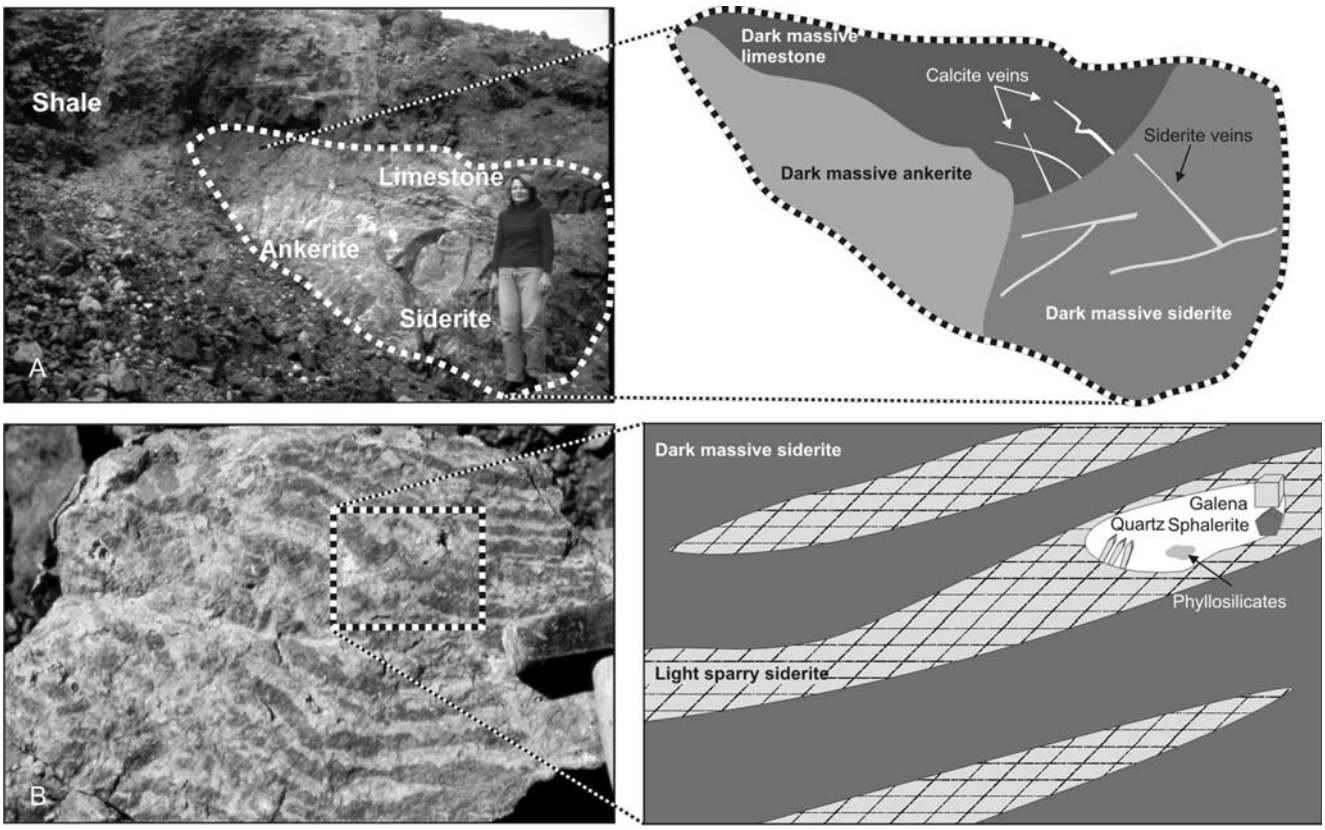

Fig. 3 Field photographs and corresponding sketches of the three main types of ore textures from the Ljubija ore deposits. **a** Dark massive siderite and ankerite hosted by dark massive limestone blocks, the Tomašica open-cast mine. **b** Zebra-banded siderite, composed of dark massive and light sparry siderite, contains cavities infilled with sparry ankerite, quartz, sulfides, and alteration phyllosilicates, the Adamuša open-cast mine. **c** Sparry siderite veins in shale, the Adamuša open-cast mine

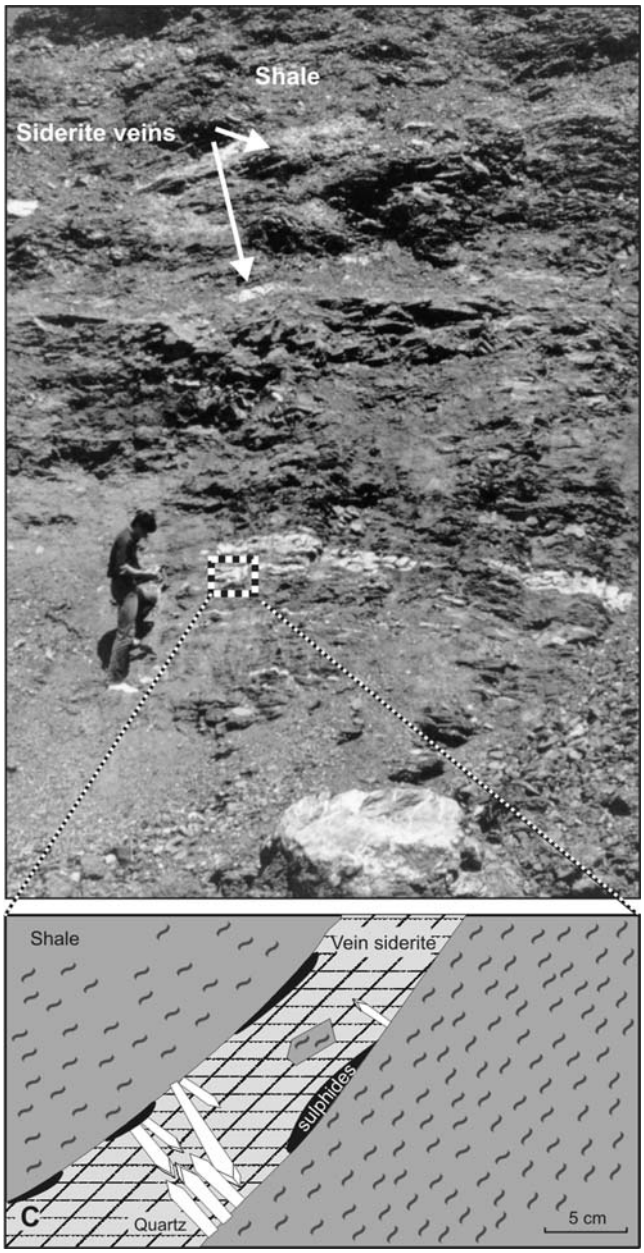

Fig. 3 (continued)

tion, moderate to high salinities (17.5–39.0 wt.% NaCl equ), and homogenization temperatures (T_h) ranging from 110°C to 260°C. Fluid inclusions within quartz from siderite veins have low homogenization temperatures (T_h=90–138°C), low to moderate salinities (2.0–22.0 wt.% NaCl equ), and NaCl-$CaCl_2$-H_2O compositions. Free CO_2 could not be detected in any fluid inclusion (Palinkaš et al. 2003). Fluid inclusions within fluorite from the Vidrenjak opencast mine are characterized by boiling phenomena characterized by coexisting liquid- and vapor-rich inclusions with homogenization temperatures within the same interval. The depth of formation, determined on the basis of pressure-temperature-composition properties of boiling fluids was between 200 and 500 m, depending whether lithostatic or hydrostatic pressure is applied (Palinkaš 1988; Borojević and Palinkaš 2001). The molar Na/Br vs. Cl/Br ratios, used as tracers of fluid origin and evolution, suggest involvement of seawater in the ore-forming processes (Palinkaš et al. 2003).

Pb isotopes in galena using the Doe–Stacey, Stacey–Kramer, and Doe–Zartman models of lead growth curve give Permo-Triassic age of mineralization (Palinkaš 1985). The sources of metals, including lead, were Paleozoic orogenic sediments leached by hydrothermal waters.

K/Ar dating of illite–smectite minerals from Carboniferous shale, the host rocks of siderite mineralization in Ljubija, was based on an assumption that these minerals lost Ar during metamorphism (Palinkaš et al. 2003). Fragments of the host shale, incorporated within siderite veins, were protected from strain and stress in the rigid sideritic matrix and preserved Ar developed after cooling. The diffusion blocking temperature of illite–muscovite minerals is around 260°C (Hunziker et al. 1986) meaning that the cooling age can be accepted as a good approximation for the time of mineralization. The determined ages for the surrounding host rock shale vary widely between 130 and 290 Ma, but the shale fragments gave values in a narrow range between 236 and 238 Ma (Palinkaš et al. 2003).

Samples and methods

Sixty-two barren and mineralized whole rock samples were collected from the Tomašica and Adamuša opencast mines. The samples were prepared and analyzed at the Institute of Mineralogy and Geochemistry of the University of Lausanne using procedures described previously (Spangenberg and Macko 1998; Spangenberg et al. 1999; Spangenberg and Herlec 2006). To remove the weathered material and any contamination from packing and handling, the rock samples were cut in slabs with a water-cooled saw. The slabs were cleaned with distilled water, analytical grade, and glass distilled acetone and ethanol and dried at 50°C for 24 h. The cleaned slabs were crushed and powdered by short grinding periods in a tungsten carbide ring grinder mill. The samples were classified as barren or mineralized according to the concentration of iron determined by X-ray fluorescence analyses of pressed whole-rock powder. Nonmineralized limestones, siltstone, and shale represent barren samples. Mineralized samples are characterized by Fe/(Fe+Ca+Mg) ratio higher than 0.03 and include Fe-enriched limestones, dark massive ankerite, dark massive siderite, zebra-banded siderite, and vein siderite. Various mineralogically and texturally homogenous subsamples were separated from hand specimens.

Mineralogical phase analyses (X-ray diffraction) were performed using a Philips PW 3040/60 X'Pert PRO powder diffractometar (45 kV, 40 mA) with CuKα monochromatized

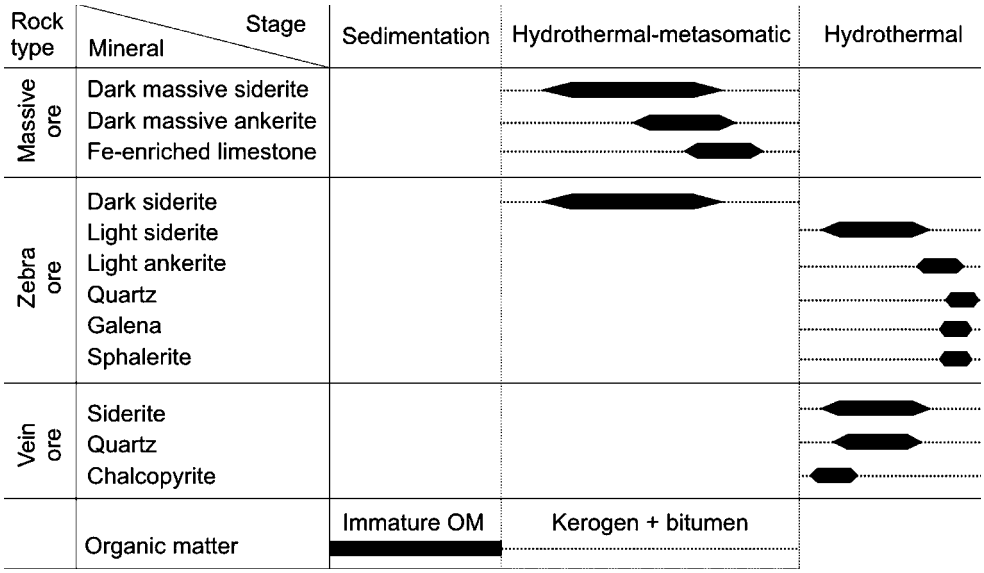

Fig. 4 Simplified paragenesis of the Ljubija mineralization

radiation (λ=1.54056 Å) and θ–θ geometry at the Department of Mineralogy and Petrography of the University of Zagreb.

Carbon and oxygen isotope compositions of mineralized and barren carbonates were determined on an automated Thermo Fischer (former Thermoquest/Finnigan, Bremen, Germany) Gasbench II preparation device connected to a Thermo Fischer Delta Plus XL isotope ratio mass spectrometer (IRMS) that was operated in the continuous helium flow mode (Révész and Landwehr 2002). CO_2 extraction was done with 100% phosphoric acid at 70°C for calcite and at 90°C for Fe carbonates and dolomite. The normalization of the measured isotope ratios to the international reference scales were performed by replicate analyses of a laboratory standard (Carrara marble) in each run. For Fe carbonate runs phosphoric acid-based corrections were done, using the fractionation equations of Das Sharma et al. (2002) and the carbonate–phosphoric acid fractionation factors reported by Rosenbaum and Sheppard (1986). The isotopic compositions are reported as δ-notation in per mil relative to Vienna-Standard Mean Ocean Water (V-SMOW) for oxygen and Vienna-Pee Dee belemnite standard (V-PDB) for carbon. The analytical reproducibility, estimated by analyses of laboratory standard (Carrara marble), was better than ±0.05‰ for $\delta^{13}C$ and ±0.1‰ for $\delta^{18}O$ (1σ).

Sulfur isotope analyses were performed on sulfides and sulfates using a Carlo Erba 1108 elemental analyzer (EA) connected to a Thermo Fischer Delta S IRMS (EA/IRMS). The sulfur isotope values are reported relative to Vienna-Canyon Diablo troilite standard (V-CDT). The reproducibility, assessed by replicate analyses of laboratory standards (pyrite, working value=6.1‰; synthetic mercury sulfide, working value=15.5‰; barium sulfate, working value=12.5‰ $\delta^{34}S$), was better than 0.2‰. Twenty-five mineralized and barren whole-rock samples were analyzed at ACTLABS (Activation Laboratories Inc., Ontario, Canada) after lithium metaborate or tetraborate fusion using inductively coupled plasma (ICP) for major elements and ICP-MS for trace elements.

Eighteen mineralized and barren whole-rock samples were selected for organic geochemical analyses. Rock powders were submitted to total organic carbon (TOC) and Rock-Eval analyses at the Humble Geochemical Services Division (Humble, TX, USA). Aliquots of samples were extracted with dichloromethane. From these aliquots, the extractable organic matter was desulfurized and fractionated by silica–alumina liquid chromatography into saturated, aromatic, and NSO compounds. Chemical characterization of the saturated and aromatic hydrocarbons was performed with an Agilent Technologies 6890 gas chromatogram coupled to an Agilent Technologies 5973 quadrupole mass selective detector (GC/MSD). Compound identifications were based on comparison of standards, GC retention time, mass spectrometric fragmentation patterns, and literature mass spectra. Compound specific C isotope analyses of saturated hydrocarbons were obtained by an Agilent Technologies 6890 GC coupled to a Thermo Fischer Delta S IRMS by a combustion (C) interface III (GC/C/IRMS) under a continuous He flow (Hayes et al. 1990). The GC was operated with the same type of column and temperature program used for GC/MSD analyses. The reproducibility was assessed by at least three replicate analyses of the same sample and ranged between 0.05‰ and 0.5‰. Insoluble organic matter (kerogen) was isolated by acidification of the extracted samples. The oven-dried residues (consisting mostly of kerogen with small amounts of quartz and clay) were analyzed for carbon and nitrogen isotopic composition using an EA/IRMS system. The isotopic compositions are reported as δ values in per mil

Table 1 Carbon and oxygen isotope composition of carbonates from the Ljubija ore deposits

Sample type	Sample	Carbonate name	Description	$\delta^{13}C$ (‰, VPDB)	$\delta^{18}O$ (‰, VSMOW)
Barren limestone	JS-LJ-01	JS-LJ-01-d	Dark massive limestone	1.6	20.6
	JS-LJ-02	JS-LJ-02-d	Dark massive limestone	1.9	20.4
	JS-LJ-03	JS-LJ-03-d	Dark massive limestone	1.1	20.8
	JS-LJ-04	JS-LJ-04-d	Dark massive limestone	1.8	20.2
	JS-LJ-08	JS-LJ-08-d	Dark massive limestone	3.8	20.3
	JS-LJ-31	JS-LJ-31-d	Dark massive limestone	−0.1	19.6
		JS-LJ-31-w	White calcite vein	−0.9	17.8
		JS-LJ-31-y	Yellowish calcite vein	−1.4	26.3
Fe-enriched limestone	JS-LJ-6a	JS-LJ-6a-w	White calcite vein	0.0	21.7
		JS-LJ-6a-d	Dark massive limestone	1.3	22.1
	JS-LJ-6b	JS-LJ-6b-w	White calcite vein	0.3	22.4
		JS-LJ-6b-d	Dark massive limestone	1.0	21.6
	JS-LJ-30	JS-LJ-30-d	Dark massive limestone	1.5	20.3
		JS-LJ-30-w	White calcite vein	0.4	23.4
		JS-LJ-30-y	Yellowish calcite vein	−1.9	28.2
	JS-LJ-33	JS-LJ-33-d	Dark massive limestone	0.5	20.1
		JS-LJ-33-t	Transparent calcite crystals	−4.4	17.7
	JS-LJ-A3	JS-LJ-A3-d	Dark massive limestone	−2.8	18.9
		JS-LJ-A3-w	White calcite vein	−3.3	18.6
Dark massive ankerite	JS-LJ-07	JS-LJ-07-w	White ankerite vein	0.0	20.9
		JS-LJ-07-g-1	Dark massive ankerite	−0.2	21.1
		JS-LJ-07-g-2	Dark massive ankerite	−0.3	21.1
		JS-LJ-07-d	Dark massive ankerite	0.3	21.3
Dark massive siderite	JS-LJ-10	JS-LJ-10-y	Yellowish siderite vein	−2.3	20.2
		JS-LJ-10-d	Dark massive siderite	−1.6	19.7
	JS-LJ-11	JS-LJ-11-w	White calcite vein	−1.3	20.0
		JS-LJ-11-d	Dark massive siderite	−1.6	21.1
		JS-LJ-11-y	Yellowish siderite vein	−2.2	20.3
	JS-LJ-14	JS-LJ-14-y	Yellowish siderite vein	−2.0	20.4
		JS-LJ-14-d	Dark massive siderite	−1.9	21.2
	JS-LJ-14a	JS-LJ-14a-d	Dark massive siderite	−2.2	20.8
		JS-LJ-14a-y	Yellowish siderite vein	−1.9	20.1
	JS-LJ-18	JS-LJ-18-w	White sparry ankerite vein	−0.9	19.6
		JS-LJ-18-d	Dark massive siderite	−0.9	21.0
		JS-LJ-18-y	Yellowish siderite vein	−1.9	21.4
	JS-LJ-35	JS-LJ-35-w	White sparry ankerite vein	−3.4	19.8
		JS-LJ-35-d	Dark massive siderite	−2.3	19.4
	JS-LJ-37	JS-LJ-37-d	Dark massive siderite	−0.8	21.0
		JS-LJ-37-w	White sparry ankerite vein	−1.9	21.2
	JS-LJ-A2	JS-LJ-A2-d	Dark massive siderite	−1.3	21.3
	JS-LJ-A5	JS-LJ-A5-g	Dark siderite	−0.8	20.0
Zebra siderite	JS-LJ-32	JS-LJ-32-w	White sparry ankerite	−2.4	18.6
		JS-LJ-32-y	Light siderite	−1.7	19.8
		JS-LJ-32-g	Dark siderite	−1.6	20.2
	JS-LJ-008	JS-LJ-008-y	Light siderite	−2.1	20.2
		JS-LJ-008-g	Dark siderite	−2.9	19.1
	JS-LJ-009	JS-LJ-009-y	Light siderite	−0.6	20.8
	JS-LJ-010	JS-LJ-010-y	Light siderite	−2.8	18.9

Table 1 (continued)

Sample type	Sample	Carbonate name	Description	$\delta^{13}C$ (‰, VPDB)	$\delta^{18}O$ (‰, VSMOW)
Zebra siderite	JS-LJ-011	JS-LJ-011-y	Light siderite	−2.5	19.4
	JS-LJ-112	JS-LJ-112-y	Light siderite	−2.5	19.5
	JS-LJ-013	JS-LJ-013-y	Light siderite	−3.0	19.3
	JS-LJ-014	JS-LJ-014-y	Light siderite	−2.8	18.9
	JS-LJ-015	JS-LJ-015-y	Light siderite	−2.3	19.3
Vein siderite	JS-LJ-34	JS-LJ-34	Vein siderite	−1.9	21.4
	JS-LJ-A6	JS-LJ-A6-b	Vein siderite	−3.0	20.6
		JS-LJ-A6-b2	Vein siderite	−3.8	19.5
White sparry ankerite	JS-LJ-33	JS-LJ-33-w	White sparry ankerite	−4.0	16.4
Alterated ankerite	JS-LJ-38	JS-LJ-38	Fine-grained white ankerite	−5.1	21.6

relative to V-PDB for carbon and air-N_2 (AIR) for nitrogen. Reproducibility of the EA/IRMS analyses, assessed by replicate analyses of a laboratory standard (glycine (−26.0‰ $\delta^{13}C$; 2.9‰ $\delta^{15}N$), urea (−43.1‰ $\delta^{13}C$; −1.4‰ $\delta^{15}N$), and USGS-24 (−16.05‰ $\delta^{13}C$)), was better than 0.1‰ for both $\delta^{13}C$ and $\delta^{15}N$.

Results and discussion

Carbon and oxygen isotope composition of carbonates

Carbon and oxygen isotope ratios are listed in Table 1 and presented in Fig. 5. The average $\delta^{13}C$ and $\delta^{18}O$ values for barren limestones (n=5) are 2.0±0.9‰ V-PDB and 20.5± 0.2‰ V-SMOW, respectively. Fe-enriched limestones ($\delta^{13}C$=0.3±1.4‰ and $\delta^{18}O$=20.4±1.1‰, n=6) are slightly depleted in ^{13}C compared to barren carbonates. The different generations of Fe carbonates display a general tendency toward lower $\delta^{13}C$ values in the following order: dark massive ankerite ($\delta^{13}C$=0.0±0.2‰ and $\delta^{18}O$=21.1± 0.2‰, n=3); dark massive siderite ($\delta^{13}C$=–1.6‰±0.5‰ and $\delta^{18}O$=20.7±0.7‰, n=8) and dark siderite from zebra ore ($\delta^{13}C$=–1.6±0.8‰ and $\delta^{18}O$=19.8±0.6‰, n=3); light siderite veins in dark massive siderite ($\delta^{13}C$=–2.1±0.2‰ and $\delta^{18}O$=20.7±0.7‰, n=5) and light siderite from zebra ore ($\delta^{13}C$=–2.3±0.7‰ and $\delta^{18}O$=19.6±0.6‰, n=9); light ankerite from zebra ore ($\delta^{13}C$=–2.4‰ and $\delta^{18}O$=18.6‰, n=1) and light ankerite from dark massive siderite ($\delta^{13}C$= –2.6±1.2‰ and $\delta^{18}O$=19.3±2.0‰, n=4); and vein siderite ($\delta^{13}C$=–2.9±0.7‰ and $\delta^{18}O$=20.8±1.4‰, n=3; Fig. 5).

Sulfur isotope composition of sulfides and sulfates

Isotopic data of sulfur minerals are presented in Table 2. The $\delta^{34}S$ values of the sulfides cover a relatively narrow range between –2.3‰ and 8.5‰ V-CDT, increasing in the following order: galena (–2.3‰ to 3.0‰), chalcopyrite (–0.8‰ to 2.3‰), sphalerite (0.4‰ to 0.8‰), and pyrite (5.4‰ to 8.5‰). No significant differences in the sulfur isotope composition of sulfides separated from dark massive siderite and zebra-banded ore were detected. The $\delta^{34}S$ value of barite samples is 9.2±0.2‰ V-CDT.

Major elements geochemistry

Major element concentrations of selected samples are given in Table 3. The SiO_2 content of carbonates varies between 0.02 and 31.68 wt.%, without significant difference between barren and mineralized samples. The Al_2O_3 content of barren and mineralized carbonates ranges from 0.02 to 6.08 wt.%. Due to variable aluminosilicate content, carbonates are divided as barren or mineralized on the basis of Fe/(Fe + Ca + Mg) ratio higher than 0.03. Positive correlations between Si, Al, Na, K, Ti, and P (correlation coefficient, r=0.87–0.99, n=21) reflect the important contribution of detrital aluminosilicates in the studied samples. Fe is positively correlated with Mn (r=0.91, n=21), and Ca shows negative correlation with Fe and Mn (r=0.61–0.75, n=21).

Rare earth elements geochemistry

The REE contents of the carbonates and associated siliciclastic rocks (Table 4) were normalized to post-Archean Australian shale (PAAS; values from Nance and Taylor 1976). The siliciclastic rocks are characterized by flat REE patterns (Fig. 6a). Total REE concentrations in studied carbonate samples are positively correlated with Al content (r=0.83, n=21). The samples with enhanced Al concentrations have flat normalized REE patterns similar to those of the surrounding shale. Since LREE preferably concentrate in the detrial aluminosilicate fraction, only the samples with low Al content were considered in the interpretation of the REE geochemistry. The barren limestones reveal the REE patterns with a weak positive Eu anomaly and a pronounced negative Ce anomaly (Fig. 6b).

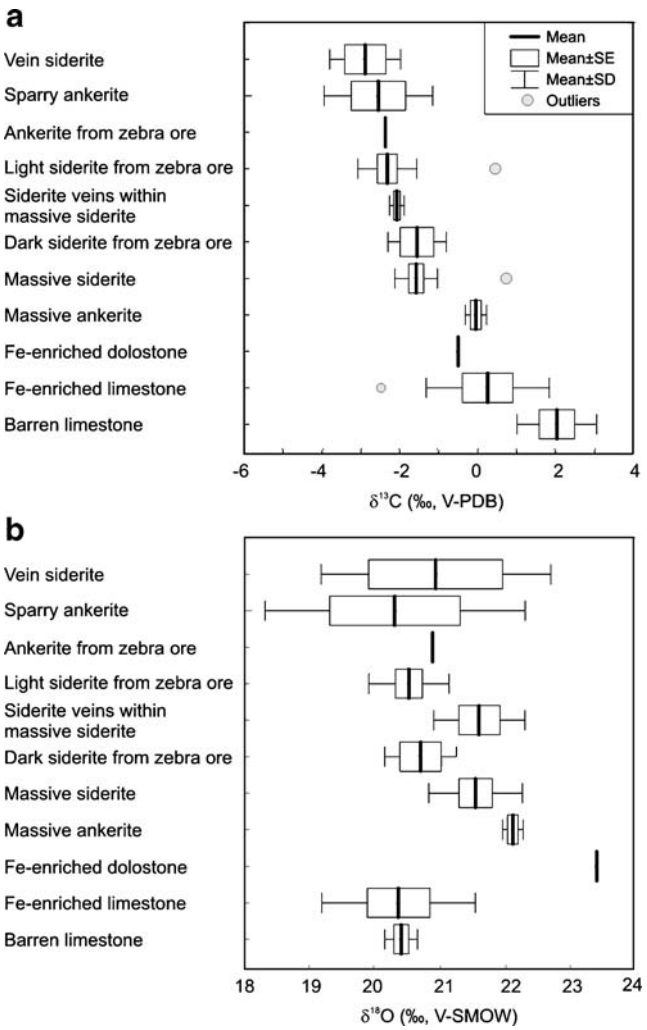

Fig. 5 Carbon and oxygen isotope data for different carbonate phases from the Ljubija deposits. **a** $\delta^{13}C$ values point to progressive metasomatic replacement of the host limestone by dark massive Fe carbonates. Light sparry siderite, ankerite, and vein siderite precipitated from hydrothermal fluids which carried bicarbonate ions depleted in ^{13}C. **b** Variations in $\delta^{18}O$ values are attributed to local discrepancies in isotopic composition and/or temperature of mineralizing fluids

Dark massive siderite and ankerite as well as Fe-enriched limestone are characterized by negative Ce anomaly (Fig. 6c–e). The Fe carbonates (dark massive siderite, light siderite, and light ankerite) separated from the zebra-banded ore display roof-shaped (convex) REE patterns with pronounced positive Eu anomalies (Fig. 6f). A negative Ce anomaly is displayed by dark massive siderite. Vein siderite possesses REE patterns with weak Ce and weak Eu anomalies (Ce/Ce^{*}=0.83–0.92; Eu/Eu^{*}=1.72–1.79) accompanied with excess of HREE over LREE (Fig. 6g).

Organic carbon content and Rock-Eval pyrolysis

The TOC content of all studied samples varies between 0.10 and 0.38 wt.% (Table 5). Barren limestones have TOC contents in the range from 0.10 to 0.38 wt.% (mean value of 0.24, n=6). The TOC contents of Fe-enriched limestones cover a narrow span between 0.20 and 0.34 wt.% (mean value of 0.27, n=3). Dark massive ankerite has TOC of 0.20 wt.%. Dark massive siderite samples are depleted in TOC (0.12 to 0.22 wt.%, mean value of 0.17, n=4). Siltstone samples have values from 0.14 to 0.22 wt.% (mean value of 0.19, n=3).

The lack of Rock-Eval S_2 (pyrolytic hydrocarbons) and low values of S_1 (free hydrocarbons) peaks (0.01 and 0.18 mg HC/g) in the Ljubija samples preclude the determination of T_{max}, HI and PI parameters, and kerogen typing. This may be attributed to high thermal maturation, extensive oxidation, or bacterial degradation of organic matter, combined with low initial organic matter content (e.g. Spangenberg and Herlec 2006). An extremely high oxygen index for siderite is expected due to low thermal stability of this mineral (Espitalié et al. 1977).

Carbon and nitrogen isotope composition of kerogens

The C-isotope composition of the kerogens ($\delta^{13}C_{ker}$) isolated from the Ljubija samples ranges from −25.9‰ to −23.3‰ V-PDB (Fig. 7a; Table 5). The mineralized carbonates ($\delta^{13}C_{ker}$ values between −25.9‰ and −24.9‰, mean value of −25.5‰, n=8) are slightly depleted in ^{13}C compared to the barren limestone (−25.8‰ to −23.3‰, mean value of −24.9‰, n=6).

Table 2 Sulfur isotope data of sulfides and sulfates from the Ljubija mineral deposits

Sample type	Sample	Mineralogy	$\delta^{34}S$ (‰, VCDT)
Dark massive siderite	JS-LJ-105-1	Pyrite	6.5
	JS-LJ-106-1	Pyrite	8.5
	JS-LJ-106-4	Pyrite	6.7
	JS-LJ-107-1	Galena	−1.3
	JS-LJ-107-2	Barite	9.3
Zebra siderite	JS-LJ-100-1	Galena	−0.5
	JS-LJ-101-1	Pyrite	7.6
	JS-LJ-104-1	Sphalerite	0.8
	JS-LJ-104-2	Chalcopyrite	2.3
	JS-LJ-104-3	Chalcopyrite	1.2
	JS-LJ-108-1	Galena	−0.4
	JS-LJ-109-2	Barite	9.2
	JS-LJ-109-3	Galena	3.0
	JS-LJ-112-1	Sphalerite	0.8
	JS-LJ-113-1	Sphalerite	0.4
	JS-LJ-113-4	Galena	−2.3
	JS-LJ-113-5	Chalcopyrite	−0.8

Table 3 Major element composition of barren and mineralized samples from the Ljubija ore deposits

Sample type	Sample	SiO_2 (wt.%)	Al_2O_3 (wt.%)	Fe_2O_3 (wt.%)	MnO (wt.%)	MgO (wt.%)	CaO (wt.%)	Na_2O (wt.%)	K_2O (wt.%)	TiO_2 (wt.%)	P_2O_5 (wt.%)	LOI (wt.%)	Total (wt.%)
Barren limestone	JS-LJ-01	23.39	5.43	1.87	0.19	0.89	35.84	0.19	1.53	0.21	0.08	28.98	98.60
	JS-LJ-02	19.29	3.75	1.52	0.22	0.91	39.51	0.14	1.12	0.14	0.07	31.42	98.09
	JS-LJ-03	25.17	5.95	2.03	0.16	1.28	33.78	0.07	1.60	0.23	0.07	27.51	97.85
	JS-LJ-04	21.19	3.37	1.35	0.13	0.93	38.58	0.17	0.93	0.13	0.06	30.91	97.76
	JS-LJ-05	2.65	0.49	0.43	0.06	1.18	52.44	0.02	0.11	0.02	0.03	42.40	99.83
	JS-LJ-08	2.99	0.37	0.67	0.08	0.60	52.66	n.d.	0.14	0.01	0.03	41.98	99.53
Fe-enriched limestone	JS-LJ-6a	5.85	0.83	3.66	0.32	2.10	46.03	0.02	0.14	0.04	0.04	39.63	98.66
	JS-LJ-6b	7.48	0.75	4.18	0.33	2.07	45.41	0.02	0.18	0.03	0.05	39.63	100.13
	JS-LJ-15	27.55	6.08	2.33	0.20	1.08	32.04	0.19	1.67	0.23	0.07	26.17	97.61
Dark massive ankerite	JS-LJ-07	4.98	0.48	16.68	1.04	8.25	28.71	n.d.	0.21	0.02	0.05	41.64	102.06
Dark massive siderite	JS-LJ-10	31.68	4.73	32.02	1.30	3.10	3.19	0.07	1.28	0.17	0.08	20.74	98.36
	JS-LJ-11	7.13	0.60	27.12	1.27	7.58	19.41	n.d.	0.27	0.03	0.03	36.03	99.47
	JS-LJ-14	11.58	0.39	50.65	1.98	3.69	1.73	n.d.	0.07	0.02	0.05	29.33	99.49
	JS-LJ-14a	12.84	0.96	48.27	1.78	4.19	1.60	n.d.	0.35	0.03	0.04	28.79	98.85
	JS-LJ-18	2.79	0.42	51.04	1.91	5.38	4.16	n.d.	0.12	0.02	0.03	33.00	98.87
Zebra siderite	JS-LJ-32-w	0.02	0.02	9.60	1.24	2.32	43.65	n.d.	n.d.	n.d.	n.d.	42.28	99.13
	JS-LJ-32-y	0.14	0.03	55.24	3.32	2.64	3.89	0.04	n.d.	n.d.	n.d.	33.29	98.60
	JS-LJ-32-d	1.83	0.45	52.64	3.19	2.63	5.13	0.05	n.d.	0.02	0.04	32.73	98.71
Vein siderite	JS-LJ-A6-d	9.47	0.49	53.91	1.66	3.34	0.52	0.02	0.03	0.02	0.02	29.30	98.78
	JS-LJ-A6-y	8.09	0.08	54.51	1.65	4.13	0.46	n.d.	n.d.	n.d.	n.d.	30.54	99.46
Sparry ankerite	JS-LJ-37	0.05	0.02	22.49	1.07	6.90	26.80	0.05	n.d.	n.d.	n.d.	41.19	98.57
Siltstone	JS-LJ-13	62.27	16.81	4.01	0.10	1.31	1.56	0.51	3.79	0.88	0.16	7.16	98.56
	JS-LJ-13b	58.67	12.24	7.39	0.25	2.34	3.97	0.26	2.88	0.68	0.13	9.79	98.60
	JS-LJ-16	46.23	14.11	4.61	0.20	4.57	8.74	0.28	3.79	0.65	0.12	15.68	98.98
Shale	JS-LJ-043	59.06	15.35	5.89	0.07	1.96	4.39	1.73	2.66	0.72	0.15	7.59	99.57

n.d. not detected

The N-isotope compositions of the kerogens ($\delta^{15}N_{ker}$) determined on barren limestones and massive siderite samples are presented in Fig. 7b and Table 5. The $\delta^{15}N_{ker}$ values of barren limestones range between 7.1‰ and 9.6‰ with the mean value of 8.6‰ (n=4). The mineralized samples are enriched in ^{15}N ($\delta^{15}N$ between 9.5‰ to 10.5‰, mean value of 10.0‰, n=2) compared to the barren samples.

Chemical characterization of hydrocarbons

Representative GC of saturated hydrocarbons from the barren and mineralized samples from the Ljubija ore deposits are shown in Fig. 8. The *n*-alkanes in the carbon number range from 11 to 25 (C_{11}–C_{24}), with a maximum between C_{13} and C_{16}, and the acyclic isoprenoids pristane (Pr) and phytane (Ph) are the dominant resolvable compounds in the GC traces of all samples (Table 6). The distribution of *n*-alkanes does not show a dominance of odd over even carbon numbers. Isoprenoids in the range C_{15} (farnesane) to C_{20} (phytane) are generally present in all samples (Table 6). High amounts of unresolved complex mixture (UCM) of hydrocarbons eluting between C_{13} and C_{32} are present in barren and slightly mineralized samples.

Nonaromatic cyclic hydrocarbons, such as terpanes and steranes, are presented in the saturated hydrocarbon fraction extracted from limestone and dark massive ankerite samples. Terpanes in the range from C_{21} to C_{33} were detected in *m/z* 191 ion chromatograms (Fig. 9). A series of steranes in the interval between C_{27} and C_{29} were detected in *m/z* 217 ion chromatograms (Fig. 10; Table 6).

Representative gas chromatograms of aromatic hydrocarbons are shown in Fig 12. The GC traces of the aromatics extracted from all samples from the Ljubija mineral deposits are dominated by methyl (M)-, ethyl (E)-, dimethyl (DM)-, trimethyl (TM)-, tetramethyl (TeM)-, and pentamethyl (PM)-naphthalenes (N). Identification of methyled naphthalens was based on ion chromatograms *m/z* 142, 156, 170, 184, and 198 and on the comparison of

Table 4 REE composition (in parts per million) and REE ratios of samples from the Ljubija ore deposits

Sample PAAS[a]	La 38	Ce 80	Pr 8.9	Nd 32	Sm 5.60	Eu 1.10	Gd 4.7	Tb 0.77	Dy 4.4	Ho 1.0	Er 2.9	Tm 0.50	Yb 2.8	Lu 0.50	Σ REE	La/Lu (N)[b]	Ce/Ce* (N)[b]	Eu/Eu* (N)[b]
JS-LJ-01	16.5	25.8	3.40	11.7	2.70	0.534	2.04	0.30	1.76	0.36	1.04	0.161	1.01	0.171	67.48	1.27	0.79	1.06
JS-LJ-02	11.8	18.9	2.50	9.27	2.22	0.495	1.89	0.27	1.66	0.33	0.92	0.137	0.83	0.149	51.37	1.04	0.80	1.13
JS-LJ-03	16.6	26.6	3.51	12.0	2.81	0.565	2.09	0.31	1.82	0.36	1.04	0.156	1.01	0.168	69.04	1.30	0.80	1.09
JS-LJ-04	17.0	26.4	3.84	14.2	3.64	0.893	2.86	0.38	2.12	0.39	1.05	0.150	0.91	0.150	73.98	1.49	0.75	1.29
JS-LJ-05	2.75	3.33	0.58	2.14	0.69	0.244	0.75	0.12	0.72	0.15	0.40	0.054	0.32	0.051	12.30	0.71	0.61	1.58
JS-LJ-08	3.12	3.95	0.76	3.22	1.04	0.576	1.10	0.16	0.92	0.17	0.44	0.054	0.33	0.049	15.89	0.84	0.59	2.51
JS-LJ-6a	3.56	4.81	0.79	3.82	1.86	1.42	2.28	0.34	1.89	0.36	0.92	0.117	0.70	0.110	22.98	0.43	0.66	3.22
JS-LJ-6b	2.93	4.00	0.69	3.47	1.78	1.45	2.15	0.30	1.68	0.32	0.82	0.105	0.61	0.101	20.41	0.38	0.65	3.46
JS-LJ-15	18.4	29.7	3.94	13.8	3.15	0.680	2.42	0.36	2.10	0.41	1.15	0.178	1.07	0.188	77.55	1.29	0.80	1.15
JS-LJ-07	1.13	1.88	0.37	2.30	2.07	1.67	2.63	0.39	2.15	0.40	0.98	0.114	0.62	0.092	16.80	0.16	0.67	3.34
JS-LJ-10	14.1	21.8	2.80	9.64	2.30	0.959	1.38	0.20	1.19	0.25	0.76	0.118	0.77	0.132	56.40	1.41	0.80	2.51
JS-LJ-11	1.98	4.38	0.84	4.65	2.26	1.70	2.19	0.35	2.03	0.38	1.03	0.136	0.83	0.125	22.88	0.21	0.78	3.56
JS-LJ-14	1.38	2.52	0.44	2.07	0.66	0.382	0.53	0.09	0.56	0.13	0.39	0.066	0.43	0.069	9.72	0.26	0.74	3.01
JS-LJ-14a	2.46	3.92	0.59	2.52	0.84	0.518	0.70	0.11	0.68	0.14	0.43	0.069	0.48	0.076	13.53	0.43	0.75	3.15
JS-LJ-18	2.53	4.37	0.72	2.86	0.92	0.598	0.85	0.13	0.87	0.18	0.51	0.076	0.51	0.082	15.21	0.41	0.74	3.15
JS-LJ-32-w	1.30	4.31	1.17	8.52	7.66	21.9	12.3	1.32	5.27	0.82	2.00	n.d.	1.12	0.140	67.83	0.12	0.80	10.52
JS-LJ-32-y	0.16	0.41	0.09	0.63	0.48	1.29	0.80	0.08	0.35	0.06	0.16	n.d.	0.10	0.016	4.63	0.13	0.79	9.71
JS-LJ-32-d	0.96	1.66	0.27	1.46	0.88	2.12	1.35	0.12	0.55	0.08	0.22	n.d.	0.15	0.020	9.84	0.63	0.75	9.07
JS-LJ-A6-d	1.15	2.51	0.34	1.49	0.84	0.502	2.04	0.46	2.76	0.52	1.49	0.223	1.26	0.175	15.76	0.09	0.92	1.79
JS-LJ-A6-y	0.05	0.14	0.03	0.31	0.68	0.424	1.94	0.47	2.72	0.51	1.47	0.219	1.26	0.169	10.39	0.00	0.83	1.72
JS-LJ-37	0.24	1.34	0.44	3.37	1.74	0.843	1.84	0.31	1.87	0.37	1.05	0.135	0.78	0.098	14.43	0.03	0.95	2.20
JS-LJ-13	30.8	58.3	6.85	22.8	5.02	0.955	3.71	0.60	3.72	0.75	2.20	0.358	2.27	0.383	138.72	1.06	0.92	1.03
JS-LJ-13b	22.1	41.2	4.93	16.8	4.27	0.946	3.28	0.52	3.22	0.64	1.86	0.309	1.97	0.339	102.38	0.86	0.91	1.18
JS-LJ-16	28.6	50.8	6.05	19.9	4.30	1.02	2.70	0.39	2.25	0.44	1.33	0.225	1.52	0.281	119.81	1.34	0.89	1.40
JS-LJ-043	29.0	59.3	7.14	26.0	4.56	0.853	3.94	0.65	4.03	0.82	2.62	0.402	2.44	0.371	142.13	1.03	0.95	0.94

n.d. not detected

[a] Chondrite-normalizing values from Nance and Taylor (1976)

[b] $(La/Lu)_N$ = fractionation of LREE from HREE; Ce and Eu anomalies are given as $(Ce/Ce^*)_N = Ce_N/[(La_N \times Pr_N)^{0.5}]$ and $(Eu/Eu^*)_N = Eu_N/[(Sm_N \times Gd_N)^{0.5}]$, where values >1 indicate positive anomaly, <1 negative anomaly, and =1 no anomaly

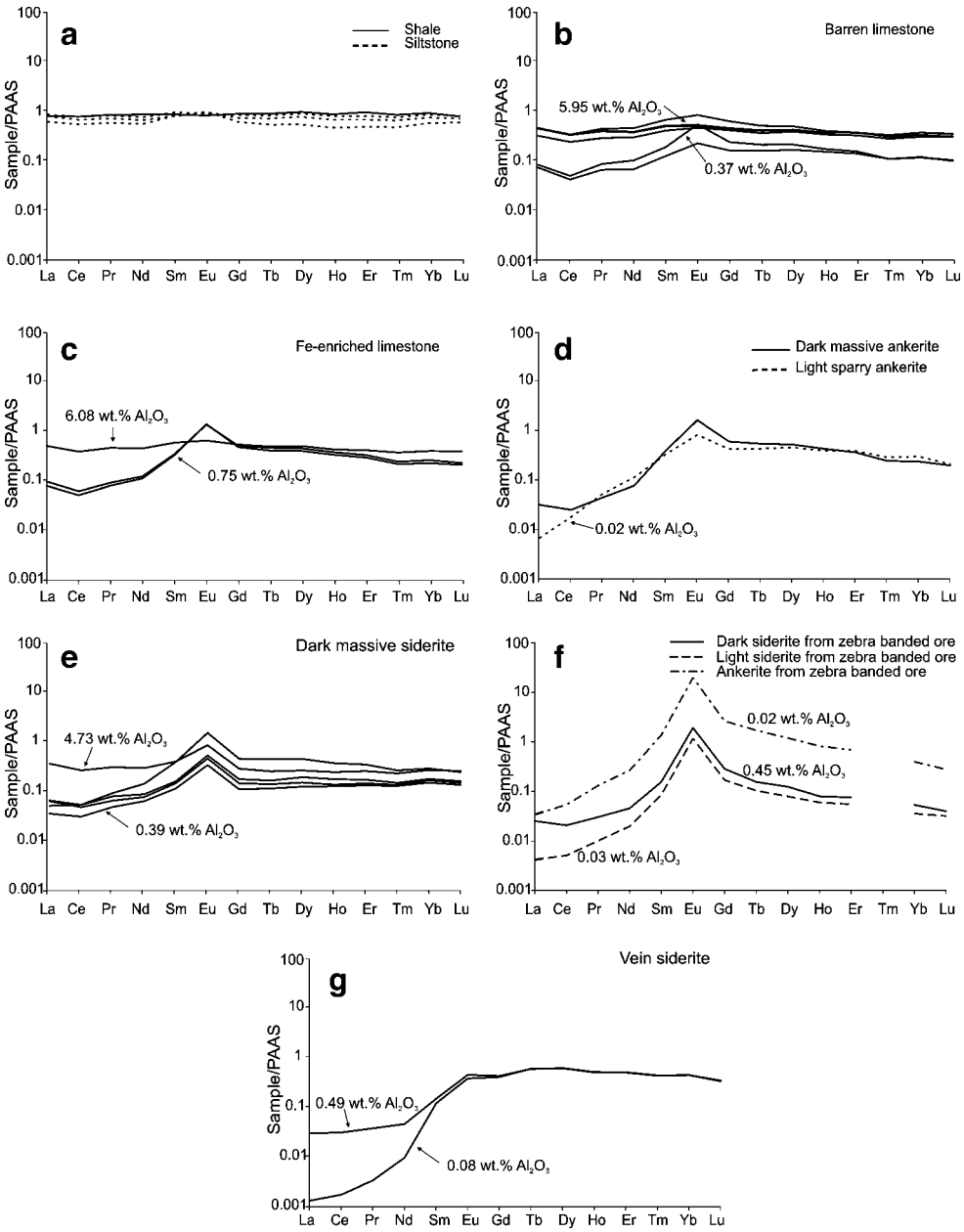

Fig. 6 The normalized REE patterns of **a** shale and siltstone, **b** barren limestone, **c** Fe-enriched limestone and dolostone, **d** dark massive ankerite and sparry ankerite, **e** dark massive siderite, **f** dark siderite, light siderite, and light sparry ankerite from zebra-banded type of ore, and **g** vein siderite

retention times with those of authentic isomers (Alexander et al. 1985; Rowland et al. 1984; Strachan et al. 1988; Forster et al. 1989; Bastow et al. 1998; Radke et al. 1994). Methyl-, dimethyl-, trimethyl-, and pentamethylnaphthalen ratios were used to characterize differences in distribution of aromatic hydrocarbons in barren and mineralized samples.

Isotopic composition of saturated hydrocarbons

The $\delta^{13}C$ values of individual alkanes cover relatively narrow range between −25.8 and −29.8‰ (Table 7). Generally, the increase in C atom number is associated with depletion in ^{13}C.

Discussion

Carbon and oxygen isotope composition of carbonates

The $\delta^{13}C$ values of barren limestones correspond well to the worldwide Phanerozoic marine carbonates values (Veizer and Hoefs 1976) and $\delta^{18}O$ values are consistent with the Carboniferous marine carbonates values (Claypool et al. 1980). The small isotopic differences between the dark massive ankerite ($\delta^{13}C$~0.0‰) and siderite ($\delta^{13}C$ approximately –1.6‰) to the light ankerite ($\delta^{13}C$ approximately –2.6‰) and light siderite ($\delta^{13}C$ approximately –2.3‰) from zebra ore suggest different stages of replacement of precursor calcite or dolomite by Fe carbonate. A

Table 5 Results of Rock-Eval analyses of whole-rock samples and isotope analyses of kerogens ($\delta^{13}C_{ker}$, $\delta^{15}N_{ker}$) from the Ljubija ore deposits

Sample type	Sample	TOC (wt.%)	Carb (wt.%)	S1	S2	S3	OI	S1/ C_{org}	$\delta^{13}C_{ker}$ (‰, VPDB)	$\delta^{15}N_{ker}$ (‰, AIR)
Barren limestone	JS-LJ-01	0.31	65.4	0.06	0.00	0.02	6	0.2	−25.8	–
	JS-LJ-02	0.25	72.6	0.06	0.00	0.01	4	0.2	−25.5	–
	JS-LJ-03	0.29	62.4	0.18	0.02	0.07	24	0.6	−25.7	7.1
	JS-LJ-04	0.38	71.9	0.09	0.00	0.10	26	0.2	−25.7	7.9
	JS-LJ-05	0.11	97.0	0.03	0.00	0.00	0	0.3	−23.3	9.6
	JS-LJ-08	0.10	96.0	0.02	0.00	0.01	10	0.2	−23.4	9.9
Fe-enriched limestone	JS-LJ-6a	0.20	93.1	0.01	0.00	0.11	55	0.0	−24.9	–
	JS-LJ-6b	0.26	89.9	0.05	0.01	0.11	42	0.2	−25.2	–
	JS-LJ-15	0.34	27.8	0.16	0.04	0.11	32	0.5	−25.9	–
Dark massive ankerite	JS-LJ-07	0.20	93.8	0.03	0.00	0.32	160	0.1	−25.8	–
Dark massive siderite	JS-LJ-10	0.22	58.7	0.01	0.00	1.25	568	0.0	−25.8	–
	JS-LJ-11	0.20	83.1	0.15	0.27	1.43	715	0.8	−25.6	–
	JS-LJ-14	0.14	87.6	0.01	0.00	4.12	2943	0.1	−25.4	9.5
	JS-LJ-14a	0.12	84.5	0.01	0.00	4.37	3642	0.1	−25.4	10.5
Siltstone	JS-LJ-13	0.22	10.7	0.06	0.02	0.08	36	0.3	−23.4	–
	JS-LJ-13b	0.14	20.0	0.03	0.00	0.11	79	0.2	−24.9	–
	JS-LJ-16	0.20	28.7	0.08	0.03	0.07	35	0.4	−24.3	–

TOC total organic carbon, *Carb* whole-rock carbonate content, *S1*, *S2* milligrams of hydrocarbons per gram of rock, *S3* milligrams of CO_2 per gram of rock, *OI* (oxygen index)=S3×100/TOC milligrams of CO_2 per gram of TOC, *SI*/C_{org} (normalized oil content)=SI×100/C_{org} milligrams of hydrocarbons per gram of TOC, – not analyzed

similar isotopic trend, with lighter stable isotope composition in paragenetically late carbonates, has been found in other comparable hydrothermal deposits (e.g., Laube et al. 1995; Spangenberg et al. 1996; Lugli et al. 2000). The small but still significant C and O isotopic differences between the Ljubija carbonate generations are explained by the progressive changes in the isotopic composition of the host carbonates and the mineralizing fluid due to mixing of different fluids, chemical exchange between rock and fluid, variations of temperature, carbon speciation, salinity, and fluid to rock ratio (e.g., Zheng and Hoefs 1993). Concentrations of various carbon species (CO_2, HCO_3^-, CO_3^{2-}, and reduced carbon) are strongly dependent on pH and oxygen fugacity (e.g., Ohmoto 1986). Therefore, the $\delta^{13}C$ variations of hydrothermal carbonates may provide valuable information on the physicochemistry of the ore-forming fluids (e.g., Zheng and Hoefs 1993). A source of isotopically light carbon could be a product of oxidation of low molecular weight hydrocarbons in host rocks (Spangenberg et al. 1996).

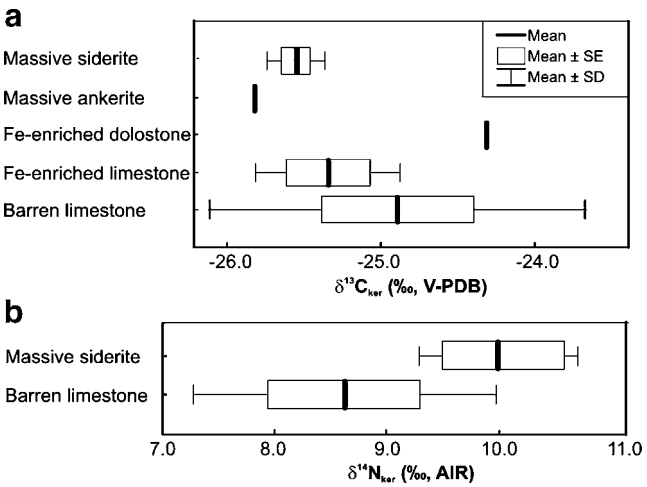

Fig. 7 Carbon and nitrogen isotopic composition of kerogens isolated from different carbonate phases from the Ljubija ore deposits. **a** Kerogens in the mineralized samples are isotopically lighter compared to the barren samples. **b** The $\delta^{15}N$ values in the barren samples, close to +8‰, suggest primary contribution of marine organic matter. The mineralized samples are enriched in ^{15}N, indicating degradation of organic material during mineralization

As the oxygen isotopic composition of the first generation of carbonates (barren limestone) is fairly uniform, the variation in the $\delta^{18}O$ values of replacing carbonates (ankerite and siderite) may be attributed to local change in composition and/or temperature of mineralizing fluids. A formation temperature of 186°C for siderite veins was calculated from $\delta^{18}O$ values of quartz–siderite pairs according to the equation of Zheng (1999). Fluid in isotopic equilibrium with both siderite and quartz at the calculated temperature should have a $\delta^{18}O$ value of 6.4‰ (Strmić Palinkaš 2004).

Physicochemical and kinetic processes of carbonate replacement may explain the development of certain

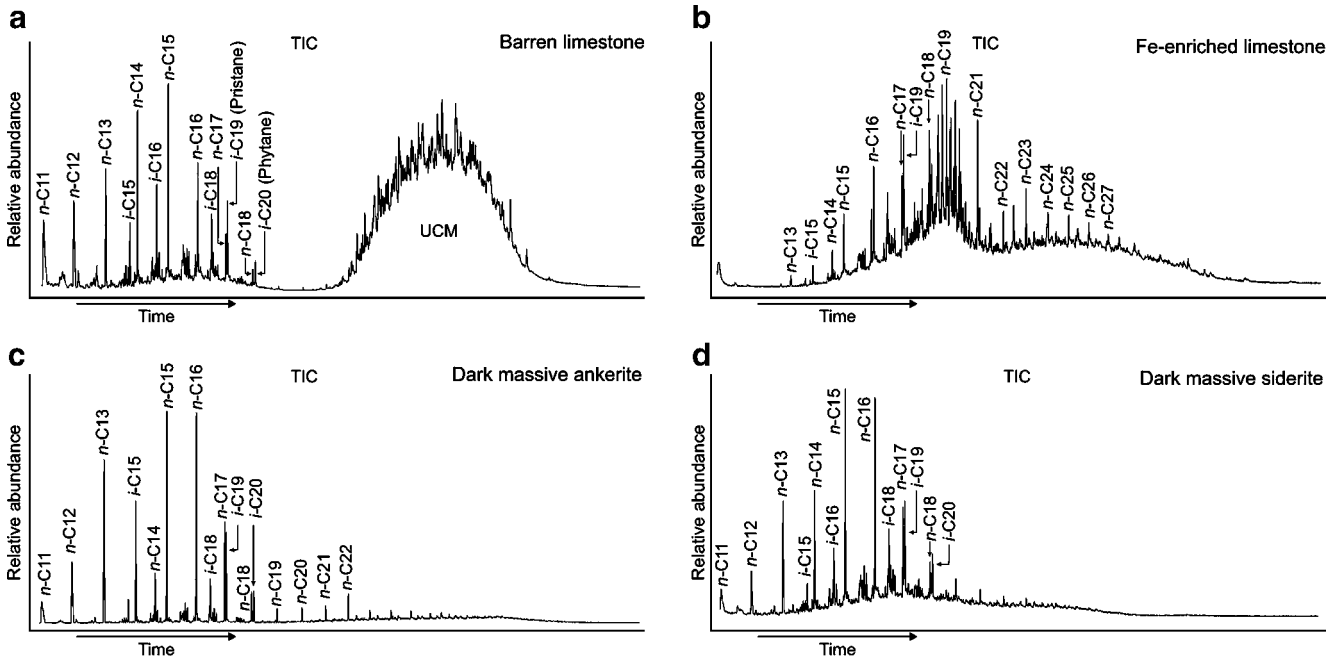

Fig. 8 Typical gas chromatography–mass selective detector total ion chromatograms (*TIC*) of saturated hydrocarbons show a dominance of normal alkanes in all sample types. The branched alkanes from the group of regular isoprenoid hydrocarbons are present in the range from farnesane (2,6,10-trimethyldodecane) to phytane (2,6,10,14 tetramethylhexadecane). **a** Barren limestone are characterized by pronounced unresolved complex mixture (*UCM*), hydrocarbon chains with up to 32 C atoms, Pr/*n*-C_{17} ratios between 1.0 and 2.8, and Ph/*n*-C_{18} ratio from 0.9 to 2.4. **b** Fe-enriched limestone has Pr/*n*-C_{17} and Ph/*n*-C_{18} ratios ranging in the intervals from 1.5 to 2.3 and from 1.1 to 1.7, respectively. **c** Dark massive ankerite (Pr/*n*-C_{17}=1.0; Ph/*n*-C_{18}= 1.4) contains hydrocarbons that range in carbon chain length from C_{11} to C_{29} (normal alkanes). **d** Dark massive siderite samples (Pr/*n*-C_{17} between 1.2 and 1.7; Ph/*n*-C_{18} between 1.0 and 2.2) have shorter hydrocarbon chains with less than 25 C atoms

textures present within the Ljubija siderite deposits. The dark massive siderite may represent a fabric retentive replacement. Such process requires simultaneous dissolution of calcite and precipitation of siderite. The volumetric dissolution rate of the replaced mineral must be equal to the volumetric precipitation rate of the replacing mineral (e.g., Garrels and Dreyer 1952; Minguez and Elorza 1994; Lugli et al. 2000). Dissolution and crystallization processes may also explain the zebra texture of the siderite ore. Neoformed replacive and displacive siderite crystals form dark and light bands in the zebra ore by feedback dissolution–crystallization mechanisms most probably triggered by a self-organization process (e.g., Lugli et al. 2000; Merino et al. 2006 and references therein).

Sulfur isotope composition of sulfides and sulfates

Sulfur isotope compositions of sulfides and sulfates were determined in order to constrain the sulfur source and mineralization temperature. The formation temperature of 246°C for the pair sphalerite–galena separated from zebra siderite (sample JS-LJ-113) is calculated according to the equations of isotope fractionation by Li and Liu (2006).

The $\delta^{34}S$ values of barite samples fall within the range of the uppermost Permian marine evaporites (Claypool et al. 1980). The fractionation factors between aqueous sulfate and sulfate minerals are very small at temperature above 100°C, and the $\delta^{34}S$ values of aqueous sulfates may be approximated by $\delta^{34}S$ values of sulfate minerals (Ohmoto 1986), suggesting that mineralization was Permian or younger. The relatively narrow range of the mostly positive $\delta^{34}S$ values of sulfides accords with thermochemical reduction of Permian seawater sulfate or contemporaneous evaporates as the main sulfur source. The Na/Br vs. Cl/Br "evaporation trend" of the fluids leached from Ljubija ore samples point to a modified Permian seawater component in the mineralization fluid (Palinkaš et al. 2003). An additional source of sulfur can be sedimentary pyrite and organically bound sulfur, whose contribution could explain the lower $\delta^{34}S$ values.

Rare earth elements geochemistry

The negative Ce anomaly observed in the barren limestone is typical for marine carbonates. Due to oxidizing conditions in seawater, Ce^{3+} is oxidized to Ce^{4+}, which is less mobile and results in Ce depletion of seawater. Therefore, marine water commonly displays a negative Ce anomaly which is then preserved in marine carbonates (e.g., Elderfield and Greaves 1982; Hu et al. 1988; Hecht et al. 1999).

Table 6 Hydrocarbon and biomarker parameter distribution of saturated fractions from barren and mineralized samples from the Ljubija ore deposits

Sample type	Sample	*n*-Alkanes (maxima)	UCM	Pr/Ph	Pr/*n*-C_{17}	Ph/*n*-C_{18}	Acyclic isoprenoids	Steranes (%)		
								C_{27}	C_{28}	C_{29}
Barren limestone	JS-LJ-01	C_{11}–C_{23} (C_{13})	–	1.88	0.99	0.99	C_{15}–C_{20}	36.0	36.9	27.1
	JS-LJ-02	C_{11}–C_{32} (C_{15})	C_{21}–C_{32}	4.14	2.80	2.18	C_{14}–C_{20}	47.7	28.1	24.3
	JS-LJ-03	C_{11}–C_{26} (C_{15})	–	2.44	2.00	1.54	C_{15}–C_{20}	–	–	–
	JS-LJ-04	C_{11}–C_{25} (C_{15})	–	3.21	1.69	2.39	C_{14}–C_{20}	–	–	–
	JS-LJ-05	C_{11}–C_{26} (C_{16})	–	2.08	1.29	0.89	C_{15}–C_{20}	–	–	–
	JS-LJ-08	C_{11}–C_{27} (C_{13})	–	2.51	1.45	0.98	C_{14}–C_{20}	–	–	–
Fe-enriched limestone	JS-LJ-6a	C_{11}–C_{28} (Pr)	C_{13}–C_{29}	1.94	1.99	1.09	C_{16}–C_{20}	–	–	–
	JS-LJ-6b	C_{11}–C_{27} (pr)	C_{14}–C_{27}	1.89	2.28	1.24	16–20	–	–	–
	JS-LJ-15	C_{11}–C_{22} (C_{15})	–	2.75	1.53	1.66	C_{14}–C_{20}	–	–	–
Dark massive ankerite	JS-LJ-07	C_{11}–C_{27} (C_{16})	–	2.56	1.03	1.36	C_{15}–C_{20}	28.3	28.7	43.0
Dark massive siderite	JS-LJ-10	C_{11}–C_{21} (C_{15})	–	3.03	1.45	1.49	C_{14}–C_{20}	–	–	–
	JS-LJ-11	C_{11}–C_{22} (C_{13})	–	2.67	1.66	1.10	C_{16},C_{17},C_{19},C_{20}	–	–	–
	JS-LJ-14	C_{11}–C_{24} (C_{15})	–	2.52	1.43	1.03	C_{15}–C_{20}	–	–	–
	JS-LJ-14a	C_{11}–C_{22} (C_{16})	–	1.82	1.44	2.19	C_{14}–C_{20}	–	–	–
	JS-LJ-18	C_{11}–C_{20} (C_{15})	–	2.64	1.23	1.26	C_{14}–C_{21}	–	–	–
Siltstone	JS-LJ-13	C_{11}–C_{25} (C_{13})	–	2.15	1.04	1.11	C_{14}–C_{16},C_{19},C_{20}	–	–	–
	JS-LJ-13b	C_{11}–C_{23} (C_{15})	–	4.92	1.41	3.00	C_{14}–C_{20}	–	–	–
	JS-LJ-16	C_{11}–C_{28} (C_{15})	–	3.26	1.33	1.57	C_{14}–C_{20}	–	–	–

– not detected, *UCM* unresolved complex mixture, *Pr* pristane, *Ph* phytane, C_x alkane with *x* carbon atoms

Massive siderite and ankerite display negative Ce anomalies inherited from their marine protoliths. In comparison to barren limestone, massive siderite and ankerite display slightly greater positive Eu anomalies suggesting a contribution from mineralizing fluids to the REE concentrations. Although hydrothermal fluids have low REE content, high-temperature chloride-rich solutions with pH below 7 may show large positive Eu anomalies (Michard 1989). In reducing, acidic high-temperature environments divalent Eu is dominant over trivalent Eu. During sorption-controlled fluid–rock interaction, the large Eu^{2+} ion can be more efficiently desorbed than its trivalent neighbors and the fluid will develop a positive Eu anomaly (Bau and Möller 1992). The pronounced positive Eu anomalies of mineralized samples in the Ljubija deposits indicate that Eu was trivalent during siderite formation, i.e., carbonates were precipitated in a low-temperature environment (<250°C) from a fluid which had received its REE signature during fluid–shale interaction in a high-temperature environment. Carboniferous shale probably served as the major source metals (iron, lead, zinc, barium).

The convex REE patterns recognized in the Fe carbonates from the zebra-banded ore are typical for fluids that have interacted with metasediments under acidic conditions (e.g., Hecht et al. 1999; Ohr et al. 1994; Lüders et al. 1993). The negative Ce anomaly preserved by dark massive siderite indicates the marine origin of its sedimentary protolith.

The LREE depletion in vein siderite suggests precipitation of siderite from a hydrothermal solution (e.g., Spangenberg et al. 1999). It is well known that ionic size, charge, and type of chemical bond control substitution of ions. Due to differences in ionic radius between Ca^{2+}, Fe^{2+}, and REE^{3+}, the REE may substitute for Ca in carbonates. HREEs are more easily incorporated in the siderite crystal lattice because they have smaller ionic radii than LREEs and higher charge than Fe^{2+} (Bau and Möller 1992). The weak Eu anomaly is attributed to precipitation from fluid that had previously reacted with limestones in a low-temperature environment (<250°C).

Carbon and nitrogen isotope composition of kerogens

The kerogens isolated from the barren and mineralized carbonates, with $\delta^{13}C$ values lower than −23.3‰, reveal the predominance of marine organic matter without significant terrestrial contribution (e.g., Lewan 1986). The isotopic composition of kerogen is affected little during maturation, unless catagenetic alteration of organic matter was appreciably above the anthracite stage or if it is affected by high-grade metamorphism. Therefore, simple thermal maturation/alteration of the kerogens cannot account for the ^{13}C

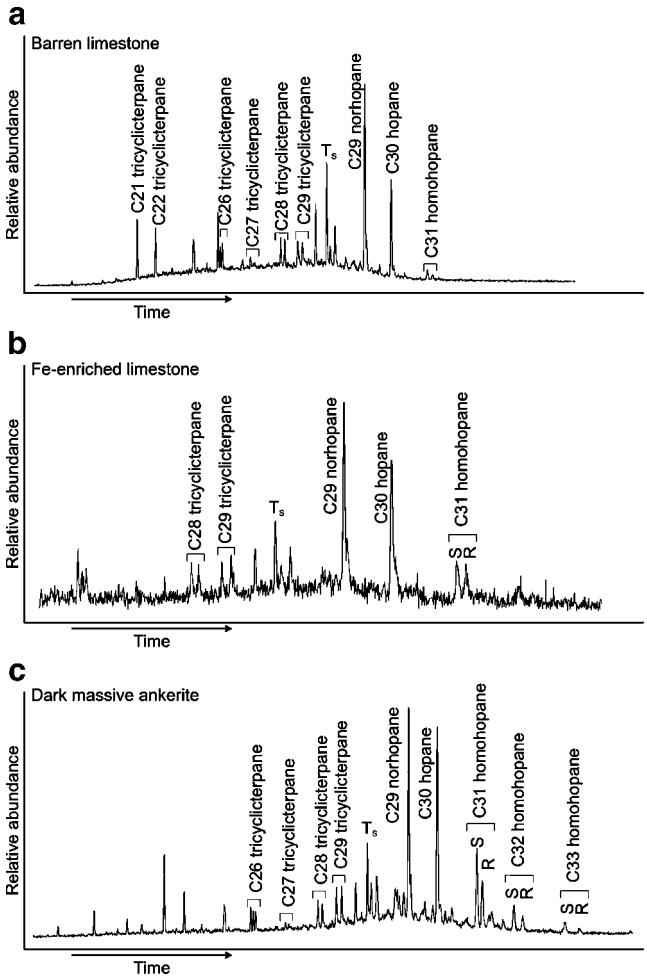

Fig. 9 Expanded ion chromatograms of *m/z*=191 showing the distribution of terpanes (cyclic alkanes derived predominantly from bacteria). **a** Barren limestones are characterized by the presence of hopanes (tricyclic terpanes with 21 to 30 C atoms) and C_{31} homohopane. **b** Fe-enriched limestone contains C_{28}–C_{30} tricyclic terpanes and C_{31} homohopane. **c** Dark massive ankerite contains hopanes and C_{31}–C_{33} homohopane. Trepanes are not recorded in the saturated fractions of dark massive siderite

depletion during mineralization (e.g., Spangenberg and Macko 1998; Schimmelmann et al. 2001).

The $\delta^{15}N_{ker}$ values of barren limestones around 0‰ suggest predominance of marine organic matter over terrestrial organic matter (e.g., Peters et al. 1978). The apparent increase of $\delta^{15}N_{ker}$ values in mineralized samples can be attributed to thermal maturation, because of the preferential release of isotopically lighter thermally less stable N-containing aromatic compounds (Bakel and Philip 1990). This may suggest that maturation of the indigenous organic matter increased due to interaction with the circulating hot mineralizing fluids (Boudou et al. 2008). It is also possible that isotopically heavier nitrogen compounds introduced by mineralizing fluids condensed on indigenous kerogens (Spangenberg and Macko 1998).

Chemical characterization of hydrocarbons

The normal alkanes in the range from *n*-C_{13} to *n*-C_{19}, recorded in the barren and mineralized sample, are typical for organic matter derived from marine plankton and algae (e.g., Tissot and Welte 1984; Hunt 1996 and references therein). The absence of UCM from siderite represents the principal difference in the normal alkanes distribution between the barren and mineralized samples. Generally, the differences in the hydrocarbon distributions can result from variation in biological sources, thermal maturity, host rock mineralogy, and degree of hydrothermal alteration (e.g., Tissot and Welte 1984). A significant UCM in the region of *n*-C_{30} has been documented in carbonate host rocks of Mississipi Valley-type deposits and has been attributed to enhanced hydrothermal alteration (Giże and Barnes 1987; Spangenberg and Macko 1998).

There is no significant difference between Pr/Ph ratios of barren and mineralized samples. With regard to biological source, organic matter derived from higher plants has high Pr/Ph ratios, generally in the range of 5 to 10. Organic matter derived from marine algal sources is characterized by lower Pr/Ph ratios, ranging from 1 to 3 (Large and Giże 1996). Therefore, the Pr/Ph ratios of 1.7 to 4.9 from Ljubija samples point to organic matter derived from marine algae. The Pr/*n*-C_{17} and Ph/*n*-C_{18} ratios decrease with increasing

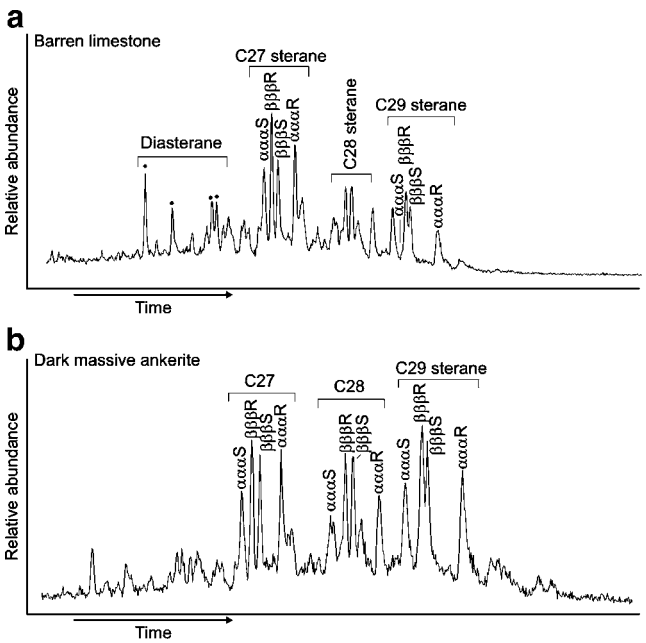

Fig. 10 Expanded ion chromatograms of *m/z*=217 showing the distribution of steranes. Steranes are C_{19} to C_{31}, three- or four-ring cyclic compounds derived from plants and animals. **a** Barren limestone contains both diasteranes and steranes. Predominance of C_{27} over C_{29} steranes is typical for hydrocarbons derived from marine organic matter. **b** Excess of C_{29} over C_{27} steranes indicates involvement of terrestrial organic matter in the extract from dark massive ankerite

Table 7 $\delta^{13}C$ values of *n*-alkanes (*n*-C_x) and isoprenoids (Pr, Ph) in samples from the Ljubija ore deposits

Sample type	Sample	$\delta^{13}C$ (‰, VPDB)												
		n-C_{11}	*n*-C_{12}	*n*-C_{13}	*n*-C_{14}	*n*-C_{15}	*n*-C_{16}	*n*-C_{17}	Pr	*n*-C_{18}	Ph	*n*-C_{19}	*n*-C_{20}	*n*-C_{21}
Barren limestone	JS-LJ-01	−29.4	−29.2	−28.5	−26.7	−28.0	−28.1	−28.3	–	−28.6		–	–	–
	JS-LJ-02	−29.1	−29.5	−29.5	−28.5	−28.4	−28.2	−27.8	−27.2	−28.1	−28.6	–	–	–
	JS-LJ-03	–	–	–	–	−27.5	−27.8	−27.8	−27.3	−28.4	−28.3	−28.1	−28.4	–
	JS-LJ-04	–	–	−28.6	−27.7	−27.7	−28.0	−28.1	−27.3	−28.6	−28.4	–		–
	JS-LJ-05	–	−27.1	−27.1	−26.7	−28.2	−28.4	−28.6	−28.5	−28.7	−29.0	−28.9	−28.9	−29.0
	JS-LJ-08	−28.4	−28.4	−28.2	−27.6	−27.5	−27.7	−27.7	–	−27.8	–	–	–	–
Fe-enriched limestone	JS-LJ-6a	–	–	–	–	−27.8	−28.4	−28.3	−27.5	−28.7	−28.7	–	–	–
	JS-LJ-6b	–	–	−28.3	−26.6	−27.7	−27.8	−28.3	–	−28.8	–	–	–	–
	JS-LJ-15	–	−28.8	−29.2	−28.3	−28.3	−28.4	−28.5	−27.9	−29.0	−28.7	–	–	–
Dark massive ankerite	JS-LJ-07	–	−28.8	−27.2	−25.8	−27.8	−28.2	−28.4	−28.0	−28.4	−29.0	–	–	–
Dark massive siderite	JS-LJ-10	−28.4	−28.6	−27.3	−26.5	−27.6	−27.9	−28.1	−27.6	−28.5	–	–	–	–
	JS-LJ-11	−29.8	−28.8	−26.8	−26.1	−27.9	−27.7	−29.0	−27.9	−29.1	–	–	–	–
	JS-LJ-14	–	–	–	−26.7	−28.3	−28.3	−28.6	–	−28.9	–	–	–	–
	JS-LJ-14a	–	–	–	−26.5	−28.3	−28.3	−28.5	–	−28.9	–	–	–	–
	JS-LJ-18	−29.2	−29.0	−29.5	−29.0	−29.5	−29.5	−29.1	−28.1	−29.1	−28.4	−27.7	–	–
Siltstone	JS-LJ-13	−28.5	−28.5	−28.5	−27.4	−28.7	−28.4	−28.1	−27.2	−28.6	–	–	–	–
	JS-LJ-13b	−28.2	−28.2	−28.1	−27.5	−28.6	−28.5	−28.3	−27.4	−28.6	–	–	–	–
	JS-LJ-16	–	−28.5	−28.7	−29.0	−28.8	−28.7	−28.6	−27.8	−29.0	−28.6	–	–	–

X number of carbons, *Pr* pristane, *Ph* phytane, – not analyzed

Fe content. The decrease in isoprenoid abundance over adjacent *n*-alkanes can be explained by thermal instability of isoprenoids relative to *n*-alkanes (Price and DeWitt 2001).

Isomerization at the C-22 position in C_{31} to C_{35} 17α(H)-hopanes is used as indicator of thermal maturity of oils and bitumens (Peters et al. 2005). The 22S/(22S + 22R) ratios for C_{31} 17α(H)-hopanes increase with increasing Fe content in limestones. The calculated 22S/(22S + 22R) ratio for dark ankerite is lower than expected (Fig. 11), suggesting mixing of indigenous and introduced hydrocarbons. The rate of 17α(H)-hopanes isomerization may be affected by lithology (Peters et al. 2005). Because indigenous and introduced hydrocarbons might originate from different rock types, the parameters based on 17α(H)-hopanes isomerization cannot be used as indicators of maturity. The $T_S/(T_M + T_S)$ parameter is commonly used for maturation assessment (Peters et al. 2005). The absence of hopane T_M and the presence of T_S suggest mature organic matter.

Isomerization at the C-14 and C-17 positions in 20S and 20R C_{29} regular steranes causes an increase in ββ/(ββ + αα) ratio (Peters et al. 2005). According to Peters et al. (2005), the ββ/(ββ + αα) ratio is independent of organic matter source. Therefore, higher ββ/(ββ + αα) ratios in ankerite compared to that observed in the barren limestone suggest that organic matter maturity increased during the mineralization. A series of steranes ranging between C_{27} and C_{29} can be used as an indicator of marine versus terestrial input of organic matter (Peters et al. 2005). In barren limestones, cholestane (C_{27}) represents 36% to 47%, ergostane (C_{28}) 28–36%, and stigmastane (C_{29}) 25% to 28% of regular steranes in the range between C_{27} and C_{29} (Table 7). Higher concentrations of C_{27} steranes relative to C_{28} and C_{29} homologs indicate the dominance of marine or aquatic algal input of organic matter. In dark massive ankerite, the higher concentration of stigmastane (43%) compared to cholestane (28%) suggests the influence of terrestrial biomass. This may suggest that the mineralizing fluids introduced hydrocarbons from terrestrial organic matter.

Methylated naphtalenes are ubiquitous constituents of sedimentary organic matter (e.g., Tissot and Welte 1984), and their distribution is controlled by variations in source, thermal stress, and biodegradation (van Aarssen et al. 1999). The differences in maturity of aromatic hydrocarbons from barren and mineralized samples, estimated with different methyled naphthalene ratios, are shown in Fig. 12. The methyl naphthalene and dimethyl naphthalene ratios increase with increasing iron content (r=0.29 and r=

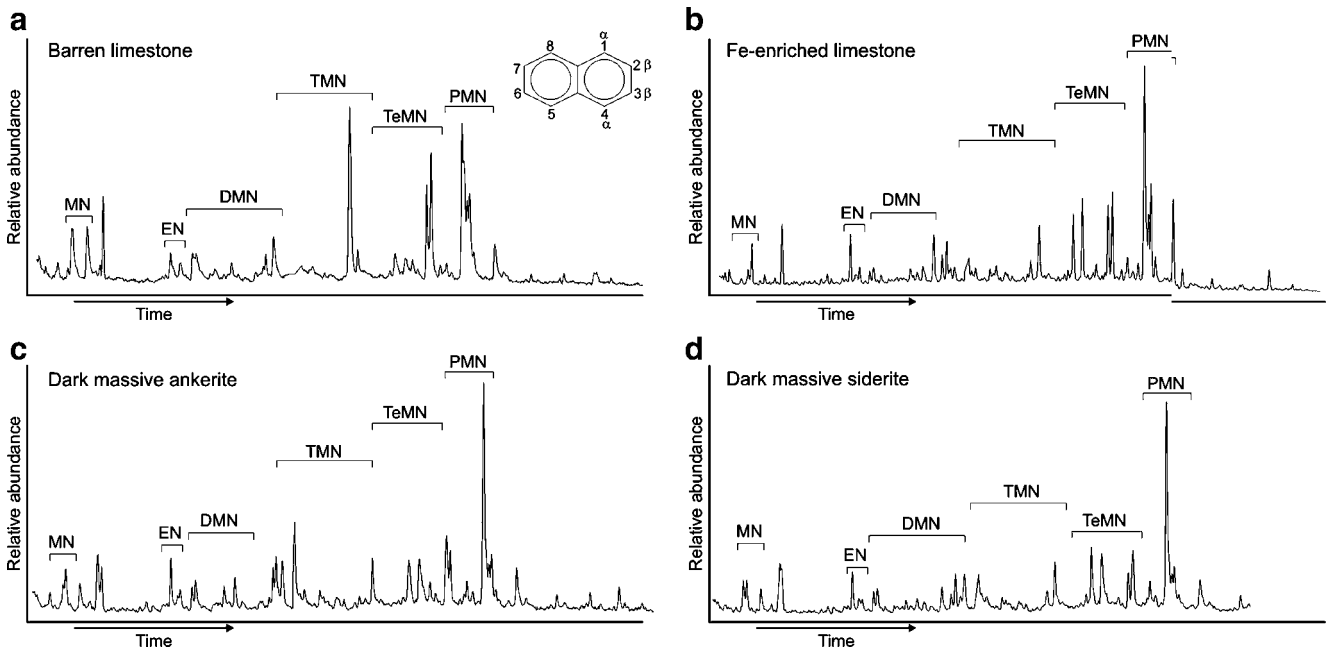

Fig. 11 Representative total ion chromatograms of aromatic hydrocarbons in **a** barren limestone, **b** Fe-enriched limestone, **c** dark massive ankerite, and **d** dark massive siderite. Methylnaphthalenes (*MN*), ethylnaphthalenes (*EN*), trimethylnaphthalenes (*TMN*), tetramethylnaphthalenes (*TeMN*), and pentamethylnaphthalenes (*PMN*) are prevalent aromatic components in all sample types

0.30, respectively, $n=18$). There is a general trend toward lower trimethyl naphthalen ($r=0.09$, $n=18$) and pentamethylnaphthalen ($r=-0.12$, $n=18$) ratios with increasing iron content. It has been shown that mature oils tend to be depleted in aromatic hydrocarbons with higher degree of alkylation (Requejo et al. 1996). Consequently, the distribution of different methyled naphthalene ratios of barren and mineralized Ljubija samples points to mixing of indigenous and introduced organic matter during mineralization processes.

Isotopic composition of saturated hydrocarbons

The decreased $\delta^{13}C$ values for higher molecular weight alkanes might be explained by ^{13}C-depletion of low molecular weight *n*-alkanes due to cracking of longer-chain hydrocarbons from a common marine phytoplanktonic origin. An alternative explanation, which is supported by the distribution of steranes and aromatic hydrocarbons, involves mixing of indigenous hydrocarbons with isotopically light alkanes introduced by mineralizing fluids.

Conclusions

1. Iron deposits within the Ljubija ore field occur as stratabound Fe carbonate ore bodies hosted by marine limestones and as siderite–sulfide veins within Carboniferous shales. Dark massive siderite and zebra-banded siderite represent two end-member types of the stratabound mineralization.
2. Stable isotopes and both inorganic and organic geochemical data are consistent with a hydrothermal–metasomatic origin and Permian age of Fe mineralization as proposed by Palinkaš (1988, 1990) and Palinkaš et al. (2003).
3. Variations in $\delta^{13}C$ values of barren and mineralized carbonates suggest progressive replacement of marine carbonates by dark massive ankerite and siderite and cannot be explained as a product of the synsedimentary event. According to $\delta^{13}C$ values, formation of the vein siderite was related to a later stage of mineralization in which mineralizing fluids, enriched in bicarbonate, penetrated the shale along brittle fractures. The formation temperature of siderite veins, calculated from the $\delta^{18}O$ values of cogenetic siderite and quartz, is ~185°C. Fluid in isotopic equilibrium with both siderite and quartz at the calculated temperature would have a $\delta^{18}O$ value of 6.4‰ V-SMOW.
4. According to the $\delta^{34}S$ values, sulfides within the zebra siderite ore precipitated at temperature of ~245°C.
5. The isotopical composition of barite ($\delta^{34}S=9.2$‰ V-CDT) and the chemical composition of the fluids leached from ore and gangue minerals indicate a contribution from Permian seawater in mineralization, which accords with a Permian age of ore formation.
6. Barren massive limestones have REE distributions typical for marine carbonates. A metasomatic origin

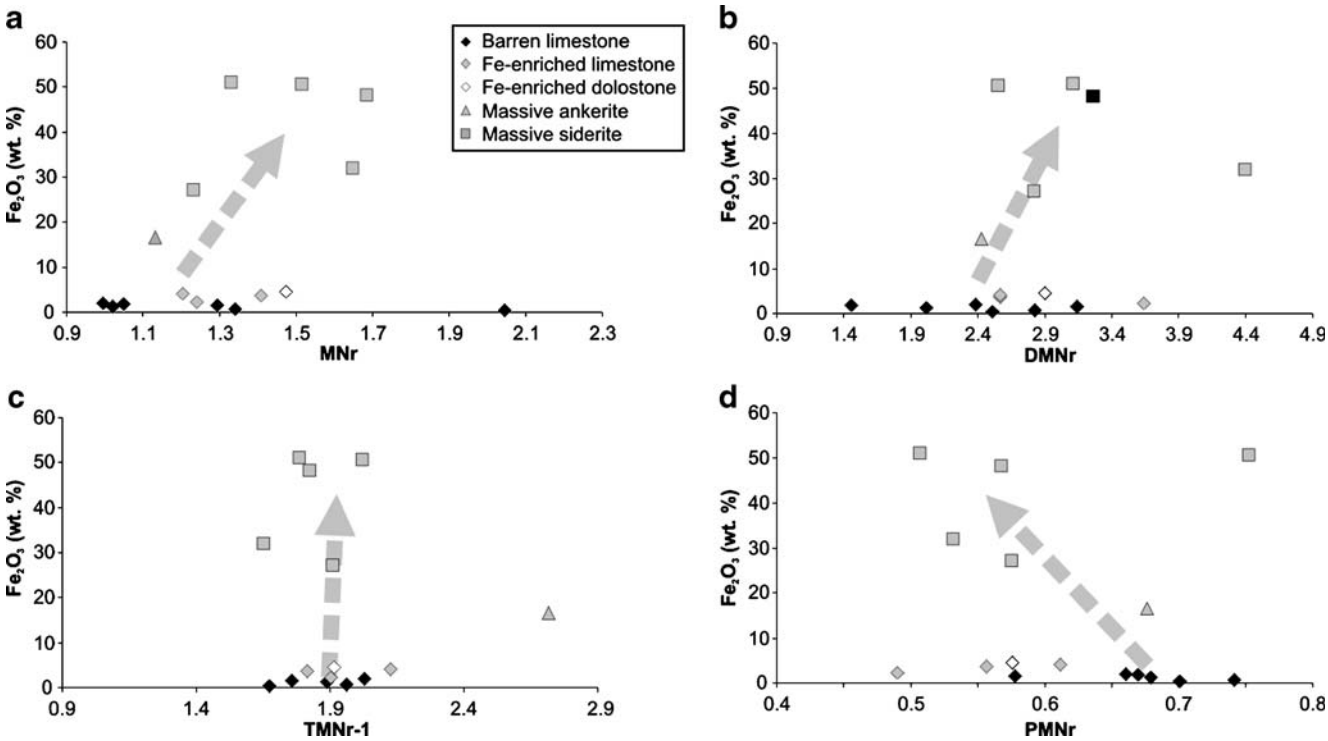

Fig. 12 Variations in organic matter maturity related with the increase in iron content of carbonates estimated on **a** methyl naphthalenes (*MN*; 2-MN/1-MN; Radke et al. 1982), **b** dimethyl naphthalenes (*DMN*; (2,6-DMN+2,7-DMN)/1,5-DMN; Radke et al. 1982), **c** trimethyl naphthalenes (*TMN*; 2,3,6-TMN/(1,4,6-TMN+1,3,5-TMN); Alexander et al. 1985), and **d** pentamethylnaphthalenes (*PMN*) ratios (1,2,4,6,7-PMN/(1,2,4,6,7-PMN+1,2,3,5,6-PMN); Bastow et al. 1998). The MN, DMN, and TMN ratios suggest increased organic matter maturity related to mineralization events. The PMN ratio decreases with increasing iron content. The absence of unambiguous interpretation of different methylnaphthalene ratios indicates mixing of indigenous and introduced organic matter during mineralization

of Fe-enriched limestone, dark massive ankerite, and dark massive siderite is suggested by the shape of their REE patterns with a preserved negative Ce anomaly and a pronounced positive Eu anomaly. Carbonates with roof-shaped REE patterns precipitated directly from a fluid which received its REE signature during fluid–rock interaction in a high-temperature acid environment. The absence of Eu anomaly in vein siderite is a consequence of precipitation in the later phase of mineralization from a fluid depleted in europium.

The distinctive features of massive siderite and zebra-banded siderite may be explained by replacement of precursor limestones by mineralizing fluids at different physicochemical conditions (e.g., temperature, acidity, and salinity).

7. The presence of geothermal gradient is supported by the REE data and stable isotope investigations. Stable isotope thermometry suggests higher temperature of formation for the stratabound siderite (zebra-banded siderite ~245°C) than for the vein siderite (~185°C).
8. Organic geochemistry data support a hydrothermal–metasomatic origin of the Ljubija ore deposits. The observed increase in $\delta^{15}N_{ker}$ values of mineralized samples can be attributed to thermal maturation during interaction with circulating hot the mineralizing fluids. An alternative explanation involves the introduction of isotopically heavier N-compounds by mineralizing fluids. The documented normal alkane distribution points to different biological sources for limestones and siderites or to hydrothermal alteration of organic matter. The biomarker and aromatic hydrocarbon distributions suggest mixing of indigenous organic matter (in limestones) and introduced organic matter (from the surrounding shale) during mineralization.

Acknowledgments This study was supported by the Swiss National Science Foundation through its program for "Scientific Co-operation between Eastern Europe and Switzerland" (Project No. 7KRPJ065483.01), the Croatian Ministry of Science, Education and Sports (Project No. 0119413), and the University of Lausanne. Reviews by Lawrence D. Meinert, Hartwig Frimmel, Bosiljka Glumac, Milica Veselinović-Williams, Ferenc Molnar, and an anonymous referee greatly improved the clarity of the manuscript. We offer a special thank to Valerie Schwab and Jošt Lavrič for their help with analytical procedures.

References

Alexander R, Kagi RI, Rowland SJ, Sheppard PN, Chirila TV (1985) The effects of thermal maturity on distribution of dimethylnaphthalenes and trimethylnaphthalenes in some ancient sediments and petroleums. Geochim Cosmochim Acta 49:385–395

Bakel AJ, Philp RP (1990) The distribution and quantitation of organonitrogen compounds in crude oil and rock pyrolysates. Org Geochem 16:353–367

Bastow TP, Alexander R, Sosrowidjojo IB, Kagi RI (1998) Pentamethylnaphthalenes and related compounds in sedimentary organic matter. Org Geochem 28:585–596

Bau M, Möller P (1992) REE fractionation in metamorphogenic hydrothermal calcite, magnesite and siderite. Mineral Petrol 45:231–246

Borojević Šoštarić S (2004) Geneza sideritno-baritno-polisulfidnih rudnih ležišta u paleozoiku Unutrašnjih Dinarida. Unpublished master thesis, University of Zagreb, Zagreb, 120 p. (in Croatian with English summary)

Borojević S, Palinkaš LA (2001) Žune ore body, boiling phenomena in hydrothermal system of Ljubija ore field, NW Bosnia. In: Ádam A, Szarka L, Szendroi G (eds) PANCARDI 2001, II. Abstracts, Sopron, Hungary, DP-5

Boudou J-P, Schimmelmann A, Aderc M, Mastalerz M, Sebiloa M, Gengembree L (2008) Organic nitrogen chemistry during low-grade metamorphism. Geochim Cosmochim Acta 72:1199–1221

Bouzenoune A, Lécolle P (1997) Petrographic and geochemical arguments for hydrothermal formation of the Ouenza siderite deposit (NE Algeria). Miner Depos 32:189–196

Cissarz A (1951) Die Stellung der Lagerstaetten Jugoslawiens im geologischen Raum. Geološki vesnik IX:23–60

Claypool GE, Holser WT, Kaplan IR, Sakai H, Zak I (1980) The age curves of sulfur and oxygen isotopes in marine sulfate, and their mutual interpretation. Chem Geol 28:199–259

Das Sharma S, Patil DJ, Gopalan K (2002) Temperature dependence of oxygen isotope fractionation of CO_2 from magnesite-phosphoric acid reaction. Geochim Cosmochim Acta 66:589–593

Đerković B, Maksimčev S, Vilovski S, Kujundžić S, Sunarić O, Hohrajn J, Kovačević R, Kačar B, Veljović R, Jojić D, Lj M, Ložajić M, Pamić J, Kapeler I, Đorđević D, Jurić M (1976) General geological map of Socialist Federal Republic of Yugoslavia, 1:100 000, sheet Prijedor. Federative Geological Survey, Belgrade

Elderfield H, Greaves MJ (1982) The rare earth elements in seawater. Nature 296:214–219

Ellmies R, Voigtländer G, Germann K, Krupenin MT, Möller P (1999) Origin of giant stratabound deposits of magnesite and siderite in Riphean carbonate rocks of the Bashkir mega-anticline, western Urals. Geol Rundsch 87:589–602

Espitalié J, LaPorte JL, Madec M, Marquis F, Leplat P, Paulet J, Boutefeu A (1977) Méthode rapide de charactériasation des roches mères de leur potential pétrolier et de leur degré d'evolution. Rev Inst Fr Pét 32:23–42

Fernández-Nieto C, Torres-Ruiz J, Subías Pérez I, Fanlo González I, González López JM (2003) Genesis of Mg–Fe carbonates from the Sierra Menera deposit (NE Spain): evidence from trace elements, REE, and stable isotope data. Econ Geol 98:1413–1426

Forster PG, Alexander R, Kagi RI (1989) Identification and analysis of tetramethylnaphthalenes in petroleum. J Chromatogr 483:384–389

Frimmel H (1988) Strontium isotopic evidence for the origin of siderite, ankerite and magnesite mineralizations in the Eastern Alps. Miner Depos 23:268–275

Garrels RM, Dreyer RM (1952) Mechanism of limestone replacement at low temperatures and pressures. Geol Soc Am Bull 63:325–380

Giže AP, Barnes HL (1987) The organic geochemistry of two Mississippi Valley-type lead-zinc deposits. Econ Geol 82:457–470

Grubić A, Cvijić R (2003) New contribution in geology and metallogeny of the Ljubija iron ore mine. Institute of Mining Prijedor, Prijedor 137 p

Grubić A, Protić Lj, Filipović I, Jovanović D (2000) New data on the Paleozoic of the Sana–Una area. In: International symposium Geology and Metallogeny of the Dinarides and the Vardar zone, Proceedings, ANURS, Banja Luka, pp 49–54

Hayes JM, Freeman KH, Popp N, Hohman CH (1990) Compound-specific isotope analysis, a novel tool for reconstruction of ancient biochemical processes. Org Geochem 16:1115–1128

Hecht L, Freiberger G, Gilg A, Grundmann G, Kostitsyn YA (1999) Rare earth element and isotope (C, O, Sr) characteristics of hydrothermal carbonates: genetic implications for dolomite-hosted talc mineralization at Göpfersgrün (Fichtelgebirge, Germany). Chem Geol 155:115–130

Hu X, Wang YL, Schmitt RA (1988) Geochemistry of sediments on the Rio Grande Rise and the redox evolution of the south Atlantic Ocean. Geochim Cosmochim Acta 52:201–207

Hunt JM (1996) Petroleum geochemistry and geology, 2nd edn. Freeman, San Francisco, p 743

Hunziker JC, Frey M, Clauer N, Dallmeyer RD, Friedrichsen H, Fleming W, Hochstrasser K, Rogwiller P, Schwander H (1986) The evolution of illite to muscovite: mineralogical and isotopic data from the Glarus Alps, Switzerland. Contrib Mineral Petrol 92:157–180

Jurić M (1971) Geologija područja sanskog paleozoika u sjeverozapadnoj Bosni. Geol Glas 11:1–146 (in Croatian)

Jurković I (1961) Minerali željeznih rudnih ležišta Ljubije kod Prijedora. Geol Vjesn 14:161–220 (in Croatian with English summary)

Katzer F (1925) Geologie Bosniens und der Hercegovina: Direkcija državnih rudarskih preduzeća, Sarajevo, 520 p

Large DJ, Giže AP (1996) Pristane/phytane ratios in the mineralized Kupferschiefer of the Fore-Sudetic Monocline, SW Poland. Ore Geol Rev 11:89–103

Laube N, Frimmel HE, Hoernes S (1995) Oxygen and carbon isotopic study on the genesis of the Steirischer Erzberg siderite deposit, Austria. Miner Depos 30:285–293

Lewan MD (1986) Stable carbon isotopes of amorphous kerogens from Phanerozoic sedimentary rocks. Geochim Cosmochim Acta 50:1583–1591

Li YB, Liu JM (2006) Calculation of sulfur isotope fractionation in sulfides. Geochim Cosmochim Acta 70:1789–1795

Lugli S, Torres-Ruiz J, Garuti G, Olmedo F (2000) Petrography and geochemistry of the Eugui magnesite deposit (Western Pyrenees, Spain). Evidence for the development of a peculiar zebra banding by dolomite replacement. Econ Geol 95:1775–1791

Lüders V, Möller P, Dulski P (1993) REE fractionation in carbonates and fluorites. In: Möller P, Lüders V (eds) Formation of hydrothermal vein deposits. Monogr Ser Miner Depos. Borntträger, Berlin, pp 133–150

Merino E, Canals A, Fletcher RC (2006) Genesis of self-organized zebra textures in burial dolomites: displasive veins, induced stress, and dolomitization. Geol Acta 4:383–393

Michard A (1989) Rare earth element systematics in hydrothermal fluids. Geochim Cosmochim Acta 53:745–750

Minguez JM, Elorza J (1994) Diagenetic volume-for-volume replacement: force of crystallization and depression of dissolution. Mineral Mag 58:135–142

Nance WB, Taylor SR (1976) Rare earth element patterns and crustal evolution—I. Australian post-Archean sedimentary rocks. Geochim Cosmochim Acta 40:1539–1551

Ohmoto H (1986) Stable isotope geochemistry of ore deposits. In: Valley JW, Taylor HP, O'Neil JR (eds) Stable isotopes in high temperature geological processes. Rev Mineral 16. Mineralogical Society of America, Chantilly, pp 491–559

Ohr M, Halliday AN, Peacor DR (1994) Mobility and fractionation of rare earth elements in argillaceous sediments: implications for dating diagenesis and low-grade metamorphism. Geochim Cosmochim Acta 58:289–312

Palinkaš LA (1985) Lead isotopes patterns in galenas from some selected ore deposits in Croatia and NW Bosnia. Geol Vjesn 38:175–189

Palinkaš LA (1988) Geokemijske karakteristike paleozojskih metalogenetskih područja. Samoborska gora, Gorski Kotar, Lika, Kordun i Banija. Unpublished doctoral thesis, University of Zagreb, Zagreb, 108 p. (in Croatian with English summary)

Palinkaš LA (1990) Siderite–barite–polysulfide and early continental rifting in Dinarides. Geol Vjesn 43:181–185

Palinkaš LA, Borojević S, Strmić S, Prochaska W, Spangenberg JE (2003) Siderite–hematite–barite–polysulfide mineral deposits, related to the early intra-continental Tethyan rifting, Inner Dinarides. In: Eliopoulos DG et al (eds) Mineral exploration and sustainable development. Millpress, Rotterdam, pp 1225–1228

Pamić J (1993) Eoalpine to Neoalpine magmatic and metamorphic processes in the northwestern Vardar zone, the easternmost Periadriatic zone and the southwestern Pannonian Basin. Tectonophysics 226:503–518

Peters KE, Sweeney RE, Kaplan IR (1978) Correlation of carbon and nitrogen stable isotope ratios in sedimentary organic matter. Limnol Oceanogr 23:598–604

Peters KE, Walters CC, Moldowan JM (2005) The biomarker guide. Volume 1: biomarkers and isotopes in the environment and human history. Volume 2: biomarkers and isotopes in petroleum exploration and earth history. Cambridge University Press, Cambridge 1132 p

Pohl W, Amouri M, Kolli O, Scheffer R, Zachmann D (1986) A new genetic model for the North African metasomatic siderite deposits. Miner Depos 21:228–233

Price LC, DeWitt E (2001) Evidence and characteristics of hydrolytic disproportionation of organic matter during metasomatic processes. Geochim Cosmochim Acta 65:3791–3826

Prochaska W (2000) Siderite and magnesite mineralizations formed during initial rifting of the Alpine cycle. In Ebner F et al (eds) Mineral resources in the Eastern Alps and adjoining areas. Mitt Osterr Geol Ges 2, pp 157–184

Radke M, Willsch H, Leythaeuser D, Teichmüller M (1982) Aromatic components in coal: relation of distribution pattern to rank. Geochim Cosmochim Acta 46:1831–1848

Radke M, Rullkötter J, Vriend SP (1994) Distribution of naphtalenes in crude oils from the Java Sea: source and maturation effects. Geochim Cosmochim Acta 58:3675–3689

Requejo AG, Sassen R, McDonald T, Denoux G, Kennicutt MC, Brooks JM (1996) Polynuclear aromatic hydrocarbons (PAH) as indicators of the source and maturity of marine crude oils. Org Geochem 24:1017–1033

Révész K, Landwehr JM (2002) $\delta^{13}C$ and $\delta^{18}O$ isotopic composition of $CaCO_3$ measured by continuous flow isotope ratio mass spectrometry. Statistical evaluation and verification by application to Devils Hole core DH-11 calcite. Rapid Commun Mass Sp 16:2102–2114

Rosenbaum J, Sheppard SMF (1986) An isotope study of siderites, dolomites and ankerites at high temperature. Geochim Cosmochim Acta 50:1147–1150

Rowland SJ, Alexander R, Kagi RI (1984) Analysis of trimethylnaphthalenes in petroleum by capillary gas chromatography. J Chromatogr 294:407–412

Schimmelman A, Boudou J-P, Lewan MD, Wintsch RP (2001) Experimental controls on D/H and $^{13}C/^{12}C$ ratios of kerogen, bitumen and oil during hydrous pyrolysis. Geochim Cosmochim Acta 32:1009–1018

Spangenberg JE, Herlec U (2006) Hydrocarbon biomarkers in the Topla–Mežica zinc–lead deposits, Northern Karavanke/Drau Range, Slovenia: paleoenvironmental at the site of ore formation. Econ Geol 101:997–1021

Spangenberg JE, Macko SA (1998) Organic geochemistry of the San Vicente zinc–lead district, eastern Pucará Basin, Peru. Chem Geol 146:1–23

Spangenberg JE, Fonboté L, Macko SA (1999) An evaluation of the inorganic and organic geochemistry of the San Vicente Mississippi Valley-type zinc–lead district, Central Peru: implications for ore fluid composition, mixing processes and sulfate reduction. Econ Geol 94:1067–1092

Spangenberg JE, Fonboté L, Sharp ZD, Hunziker J (1996) Carbon and oxygen isotope study of hydrothermal carbonates in the zinc–lead deposits of the San Vicente district, central Peru: a quantitative modeling on mixing processes and CO_2 degassing. Chem Geol 133:289–315

Strachan MG, Alexander R, Kagi RI (1988) Trimethylnaphthalenes in crude oils and sediments: effects of source and maturity. Geochim Cosmochim Acta 52:1255–1264

Strmić Palinkaš S (2004) Organic and inorganic geochemistry of Ljubija mineral deposits, NW Bosnia. Unpublished master thesis, University of Zagreb, Zagreb, 120 p

Šarac M (1981) Metalogenetske karakteristike rudonosne oblasti Ljubije. Unpublished doctoral thesis, University of Belgrade, Belgrade, 135 p (in Serbian)

Tissot BP, Welte DH (1984) Petroleum formation and occurrence. Springer, Berlin 538 p

Tomljenović B (2002) Strukturne značajke Medvednice i Samoborskog gorja. Unpublished Ph.D. thesis, University of Zagreb, Zagreb, 208 p (in Croatian with English summary)

Torres-Ruiz J (2006) Geochemical constraints on the genesis of the Marquesado iron ore deposits, Beltic Cordillera, Spain: REE, C, O and Sr isotope data. Econ Geol 101:667–677

van Aarsen BGK, Bastow TP, Alexander R, Kagi RI (1999) Distribution of methylated naphtalenes in crude oils: indicators of maturity, biodegradation and mixing. Org Geochem 30:1213–1227

Veizer JD, Hoefs J (1976) The nature of $^{18}O/^{16}O$ and $^{13}C/^{12}C$ secular trends in sedimentary carbonate rocks. Geochim Cosmochim Acta 40:1387–1395

Zheng YF (1999) Oxygen isotope fractionation in carbonate and sulfate minerals. Geochem J 33:109–126

Zheng YF, Hoefs J (1993) Carbon and oxygen isotopic covariations in hydrothermal calcites. Miner Depos 28:79–89